TECHNOLOGICAL UNIVERSITY DELFT

DEPARTMENT OF AERONAUTICAL ENGINEERING

Report VTH-124

THEORETICAL AND EXPERIMENTAL INVESTIGATIONS
OF INCOMPRESSIBLE LAMINAR BOUNDARY LAYERS
WITH AND WITHOUT SUCTION

Ph.D THESIS

J.L. van INGEN

DELFT
the NETHERLANDS

OCTOBER, 1965

This PDF-file contains chapter 9:

Stability and transition

9.   Stability and transition.

9.1.   Introductory remarks.

In the preceding chapters laminar boundary layers have been discussed
only. It is known from experiments however, that solutions of the laminar
boundary layer equations cannot always be realised in practice because
transition to turbulent flow may occur. Fig. 3.3 for instance showed a
comparison with experimental results of Blasius' theory for the laminar
boundary layer on a flat plate. It is seen that the theory is confirmed
by experiments only when the leading-edge of the plate has not been
disturbed by a tripping wire and if only those stations on the plate
are considered for which the Reynoldsnumber $\frac{Ux}{\nu}$ is less than 3×10^6.
At higher Reynoldsnumbers or when the flow is disturbed a turbulent
boundary layer is found. From detailed experiments by Schubauer and
Skramstad [87] on a smooth plate in a wind tunnel with a degree of
turbulence less than $0.1^o/o$ it is known that the flow is completely
laminar when $\frac{Ux}{\nu}$ is less than 2.8×10^6 and fully turbulent for
$\frac{Ux}{\nu} > 3.9 \times 10^6$. For intermediate values of $\frac{Ux}{\nu}$ a transition region
occurs where the flow passes from laminar to turbulent. A similar
behaviour is shown by the flow around airfoil sections or through pipes.
Although the phenomenon of transition has been known already since
Reynolds' famous experiments on pipe flow in 1883 [88] the mechanism
of transition is not yet completely understood. Neither is it possible
to predict theoretically for an arbitrary body the position where
transition will occur.
For a long time there have been two conflicting opinions about the
mechanism of transition. One school of thought supposes that
disturbances in the flow outside the boundary layer cause fluctuations
inside the boundary layer which lead to local and instantaneous separation
followed by transition (Taylor [89]). A different explanation is given
by the so called stability theory as developed by Rayleigh, Tollmien,
Schlichting, Lin, etc. (see [90] and [7], chapter 16).
In this theory it is shown that small harmonic disturbances in the
boundary layer may become unstable and amplify. It is supposed that
these disturbances cause transition as soon as they have gained a

sufficient amplification. The unstable oscillations, predicted by the stability theory were discovered in wind tunnel experiments on the boundary layer of a flat plate by Schubauer and Skramstad in 1940 [87]. It was found that the stability theory is valid only if the degree of turbulence in the airstream is less than $0.1^{\circ}/o$. For high turbulence levels Taylor's theory is more appropriate. In 1951 the existence of unstable oscillations was also shown in free flight by Malotaux et al. [91]. In the free atmosphere and in modern low speed wind tunnels the degree of turbulence is considerably less than $0.1^{\circ}/o$ and it is commonly accepted now that under these circumstances transition on smooth bodies - at least initially - is governed by the stability theory. An exception should be made for cases where the laminar boundary layer separates from the surface due to an adverse pressure gradient. It may be possible that a short distance upstream of the separation point Taylor's transition mechanism is the relevant one. Also transition in the separated layer may be governed by a different mechanism.

This theory shows under which circumstances the laminar boundary layer may become unstable and predicts the initial growth of the disturbances. Since most of the existing theories are linearised by assuming small disturbances they cannot describe the complete transition to the irregular turbulent flow with relatively large disturbances.

Our knowledge of transition has been steadily enlarged however through experiments starting with the investigations by Schubauer and Skramstad. A review of this work may be found in [29]. Some recent results have been described by Hinze et al. [92].

From the experiments it is known that in the transition region suddenly "turbulent spots" are generated. These spots grow and merge as they move downstream until finally at a certain position the flow is fully turbulent [93]. According to Klebanoff and Tidstrom [94] the spots seem to develop from threedimensional concentrations of disturbance energy in the originally two-dimensional disturbance waves.

In the first few sections of the present chapter the main principles and results of linear stability theory will be collected for later use. In the final sections it will be shown that the stability theory may be used to develop a semi-empirical method for the calculation of the

transition position on smooth bodies in an airstream with low degree of turbulence. Throughout the present work it is assumed that surface roughness is so small that it will have no influence on transition.

9.2. Principles of linear stability theory.

9.2.1. General.

The stability theory considers a given laminar main flow upon which small disturbances are superimposed. It is assumed that both the undisturbed and the disturbed flow satisfy the Navier-Stokes equations. After linearisation a perturbation equation is obtained which under certain circumstances may possess unstable solutions. It is found that important factors determining the stability or instability are:

the shape of the boundary layer velocity profile

the Reynoldsnumber $\frac{U\delta^{\ast}}{\nu}$ and

the frequency or wavelength of the disturbances.

9.2.2. The Orr-Sommerfeld equation.

In what follows a two-dimensional flow is considered which is subjected to a two-dimensional disturbance. It is possible to omit three dimensional disturbances since, according to Squire [95], the instability of incompressible boundary layer flows is initially determined by the two dimensional disturbances. For the stability investigation it is assumed that the u-velocity component of the undisturbed main flow depends only on the wall distance y and that the v component is zero; the pressure p only depends on the streamwise coordinate x. These assumptions hold exactly for pipe- or channel flow and also with a good approximation for boundary layers because here u changes much more rapidly with y than with x. (Pretsch [96]).

On the main flow a disturbance is superimposed with velocity components u'(x,y,t) and v'(x,y,t); the fluctuating pressure component is p'(x,y,t). Hence the combined flow is given by

$$u^{\ast}(x,y,t) = u(y) + u'(x,y,t)$$

$$v^{\ast}(x,y,t) = \qquad\quad v'(x,y,t) \qquad\qquad\qquad (9.1)$$

$$p^{\ast}(x,y,t) = p(x) + p'(x,y,t)$$

If (see for instance $[7]$, chapter 16)

   a) equations (9.1) are introduced into the Navier-Stokes equations
      (2.1) and (2.2) and the continuity equation (2.3);

   b) the resulting equations are linearised in the disturbance
      components;

   c) it is observed that also the undisturbed flow should fulfil
      equations 2.1 - 2.3;

   d) the fluctuating pressure component p' is eliminated from two of
      the resulting expressions;

the following equations remain:

$$\frac{\partial^2 u'}{\partial t \partial y} - \frac{\partial^2 v'}{\partial t \partial x} + u\left(\frac{\partial^2 u'}{\partial x \partial y} - \frac{\partial^2 v'}{\partial x^2}\right) + v'\frac{\partial^2 u}{\partial y^2} =$$

$$\nu\left(\frac{\partial^3 u'}{\partial x^2 \partial y} + \frac{\partial^3 u'}{\partial y^3} - \frac{\partial^3 v'}{\partial x^3} - \frac{\partial^3 v'}{\partial x \partial y^2}\right) \qquad\qquad (9.2)$$

$$\frac{\partial u'}{\partial x} + \frac{\partial v'}{\partial y} = 0 \qquad\qquad\qquad (9.3)$$

Now a periodic disturbance is assumed with a stream function ψ defined
by

$$\psi(x,y,t) = \varphi(y)e^{i(\bar{\alpha}x - \bar{\beta}t)} \qquad\qquad\qquad (9.4)$$

which, using

$$u' = \frac{\partial \psi}{\partial y} \quad \text{and} \quad v' = -\frac{\partial \psi}{\partial x} \qquad\qquad\qquad (9.5)$$

directly satisfies the continuity equation (9.3). Since (9.2) and (9.3)
are linear in the fluctuating quantities more general periodic
disturbances may be obtained by superposition of a number of components
of the form (9.4).

In the expression (9.4) it is assumed that $\bar{\alpha}$ is a real quantity; it
determines the wave length λ of the disturbance by $\lambda = \dfrac{2\pi}{\bar{\alpha}}$; $\bar{\beta}$ is

complex with $\overline{\beta} = \beta_r + i\,\beta_i$ where $\dfrac{\beta_r}{2\pi}$ is the frequency of the disturbance.
The sign of β_i determines whether the disturbance is stable or unstable.
For stable or unstable disturbances β_i is negative or positive
respectively; neutrally stable disturbances correspond to $\beta_i = 0$. The
amplitude function $\varphi(y)$ is complex and is assumed to depend on y only.
Furthermore use will be made of

$$\overline{c} = c_r + i\,c_i = \frac{\beta_r}{\overline{\alpha}} + i\,\frac{\beta_i}{\overline{\alpha}} \tag{9.6}$$

the sign of c_i again determines the stability of the disturbance; c_r
is the wave speed.

Using (9.4) and (9.5) equation (9.2) may be reduced to

$$(u-\overline{c})\left[\frac{\partial^2\varphi}{\partial y^2} - \overline{\alpha}^2\varphi\right] - \frac{\partial^2 u}{\partial y^2}\,\varphi = -\frac{i\nu}{\overline{\alpha}}\left[\frac{\partial^4\varphi}{\partial y^4} - 2\,\overline{\alpha}^2\frac{\partial^2\varphi}{\partial y^2} + \overline{\alpha}^4\varphi\right] \tag{9.7}$$

This equation can be written in non-dimensional form by using the
velocity U at the edge of the boundary layer and the displacement
thickness. δ^{*} as reference velocity and -length respectively. The result
is

$$\left(\frac{u}{U} - \frac{\overline{c}}{U}\right)\left[\frac{\partial^2\varphi}{\partial y^2}\frac{\delta^{*}}{U} - (\overline{\alpha}\delta^{*})^2\,(\frac{\varphi}{U\delta^{*}})\right] - \frac{\partial^2 u}{\partial y^2}\frac{\delta^{*2}}{U}\frac{\varphi}{U\delta^{*}} =$$

$$\frac{-i}{(\alpha\delta^{*})\,\frac{U\delta^{*}}{\nu}}\left[\frac{\partial^4\varphi}{\partial y^4}\frac{\delta^{*3}}{U} - 2\,(\overline{\alpha}\delta^{*})^2\,\frac{\partial^2\varphi}{\partial y^2}\frac{\delta^{*}}{U} + (\overline{\alpha}\delta^{*})^4\,\frac{\varphi}{U\delta^{*}}\right] \tag{9.8}$$

Equation (9.7) or (9.8) is known as the Orr-Sommerfeld equation. It
is homogeneous in φ and hence admits the solution $\varphi = 0$; this of
course represents the undisturbed flow. The stability investigation
is concerned with non-zero solutions satisfying equation (9.7) or (9.8)
together with some boundary conditions. These solutions are found by
solving the resulting eigenvalue problem. This will not be pursued
further here; extensive reviews may be found in [7, 29, 90].
In the following sections only those results of stability theory will
be presented which are used in the remainder of the present work.

9.2.3. The stability diagram.

For a given laminar boundary layer $\dfrac{U\delta^{*}}{\nu}$ and the velocity profile $\overline{u}\left(\dfrac{y}{\delta^{*}}\right)$ are

known. Then in equation (9.8) $\overline{\alpha}\delta^{*}$, $\dfrac{c_r}{U}$ and $\dfrac{c_i}{U}$ remain as parameters. Usually

$\dfrac{c_r}{U}$ and $\dfrac{c_i}{U}$ are replaced by $\dfrac{\beta_r}{U^2}$ and $\dfrac{\beta_i\delta^{*}}{U}$ using the following expressions.

$$\frac{c_r}{U} = \frac{\beta_r \nu}{U^2} \cdot \frac{1}{\overline{\alpha}\delta^{*}} \cdot \frac{U\delta^{*}}{\nu} \qquad\qquad (9.9)$$

and
$$\frac{c_i}{U} = \frac{\beta_i \delta^{*}}{U} \cdot \frac{1}{\overline{\alpha}\delta^{*}} \qquad\qquad (9.10)$$

Now, when a value for one of these parameters is assumed (for instance $\overline{\alpha}\delta^{*}$) the values of the other ones may be determined for which (9.8) allows non-zero solutions. Results of these calculations are usually presented in an $\overline{\alpha}\delta^{*} - \dfrac{U\delta^{*}}{\nu}$ plane: the "stability diagram". As an example fig. 9.1 shows the stability diagram for the flat plate boundary layer. The curve for $\dfrac{\beta_i \delta^{*}}{U} = 0$ denotes the neutrally stable disturbances. Inside the loop β_i is positive and outside negative. This means that unstable disturbances will be found only for combinations of $\overline{\alpha}\delta^{*}$ and $\dfrac{U\delta^{*}}{\nu}$ inside the loop. Below a certain value of $\dfrac{U\delta^{*}}{\nu}$ there are no values of $\overline{\alpha}\delta^{*}$ for which unstable disturbances are possible; this value of $\dfrac{U\delta^{*}}{\nu}$ is called the critical Reynoldsnumber.

The Orr-Sommerfeld equation (9.8) has been obtained for parallel flows only where $u(y)$ - and hence $\dfrac{u}{U}\left(\dfrac{y}{\delta^{*}}\right)$ and $\dfrac{U\delta^{*}}{\nu}$ - do not change with x. It is general practice to apply results of stability calculations also to flows where $u(y)$ changes slowly with x. This implies that at each station x the actual flow is replaced by a parallel flow with the same non-dimensional velocity profile $\dfrac{u}{U}\left(\dfrac{y}{\delta^{*}}\right)$ and Reynoldsnumber $\dfrac{U\delta^{*}}{\nu}$.

For a similar boundary layer the "shape of the velocity profile" $\dfrac{u}{U}\left(\dfrac{y}{\delta^{*}}\right)$ is independent of x and hence the same stability diagram applies at all values of x. If now a disturbance with a constant value of $\dfrac{\beta_r \nu}{U^2}$ is considered which is convected downstream with the flow, it follows

- because $\frac{U\delta^*}{\nu}$ increases with x - that the disturbance may at first be
stable, then become unstable and finally become stable again. The same
happens for non-similar boundary layers where however the stability
diagram changes with x.

It can be seen from the Orr-Sommerfeld equation (9.8) that the stability
diagram depends on the shape of the velocity profile. It turns out that
the curvature of the profile is very important: profiles with a point
of inflexion have a much lower critical Reynoldsnumber and hence are
much less stable than velocity profiles without inflexion point
(fig. 9.2). Moreover, the height of the unstable loop is finite when
$\frac{U\delta^*}{\nu} \longrightarrow \infty$ for velocity profiles with an inflexion point while the
height tends to zero if there is no inflexion point. Hence it follows
that factors determining the occurrence of an inflexion point have much
influence on stability and hence on transition.

An inflexion point occurs if $\frac{\partial^2 u}{\partial y^2}$ at the wall is positive. From the first
compatibility condition at the wall (equation 2.10) it follows that
$\left(\frac{\partial^2 u}{\partial y^2}\right)_o$ depends on the pressure gradient term $U\frac{dU}{dx}$ and the suction
velocity v_o. An "adverse" pressure gradient $(\frac{dU}{dx} < 0)$ or blowing
$(v_o > 0)$ tend to make $\left(\frac{\partial^2 u}{\partial y^2}\right)_o > 0$ and hence are destabilising factors.
A "favourable" pressure gradient $(\frac{dU}{dx} > 0)$ or suction $(v_o < 0)$ tend
to make $\left(\frac{\partial^2 u}{\partial y^2}\right)_o < 0$ and hence are stabilising factors. This point will
be discussed further in section 9.3.

9.2.4. The amplification factor.

It was shown in section 9.2.3. that the amplification or damping of
disturbances in the boundary layer is determined by the magnitude of β_i.
In what follows an equation will be derived which governs the growth
of the amplitude of the disturbances. This equation follows from the
expression (9.4) for the stream function. Of course, only the real
part of the stream function ψ_r is physically significant.
From (9.4), together with $\varphi = \varphi_r + i\,\varphi_i$, it follows that

$$\psi_r = e^{\beta_i t} \left[\varphi_r \cos(\overline{\alpha}x - \beta_r t) - \varphi_i \sin(\overline{\alpha}x - \beta_r t) \right]$$

or denoting $\dfrac{\varphi_r}{\varphi_i}$ by tg γ

$$\psi_r = -e^{\beta_i t} \frac{\varphi_i}{\cos \gamma} \sin (\overline{\alpha}x - \beta_r t - \gamma) \qquad (9.11)$$

For the velocity components u' and v' of the disturbance similar
expressions are found. Because φ and hence γ depend only on y the
amplitudes a and a + da for a fixed value of y at times t and t + dt
are related by

$$d(\ln a) = \beta_i \, dt \qquad (9.12)$$

Hence if the amplitude for the neutral oscillation at time t_o is denoted
by a_o, the amplitude at a later time t follows from

$$\ln \frac{a}{a_o} = \int_{t_o}^{t} \beta_i \, dt \qquad (9.13)$$

or $\qquad \dfrac{a}{a_o} = e^{\sigma_a}$ where $\qquad \sigma_a = \displaystyle\int_{t_o}^{t} \beta_i \, dt \qquad (9.14)$

In what follows σ_a will be called the "amplification factor".
For parallel flows the parameter β_i in (9.14) is constant but it may
vary with x for non-parallel flow.
Since the integration variable t in (9.14) is a little obscure for
instability calculations in boundary layers a change will be made to
the variable x by using

$$\frac{dx}{dt} = c_r \qquad (9.15)$$

This means that a disturbance is followed on its way downstream. Using
(9.15) equation (9.14) for σ_a may be written as

$$\sigma_a = \int_{x_o}^{x} \frac{\beta_i}{c_r} \, dx$$

or after introducing convenient non-dimensional quantities

$$\sigma_a = \frac{U_\infty c}{\nu} \cdot 10^{-6} \int_{\bar{x}_o}^{\bar{x}} T.\bar{U}\, d\bar{x} \tag{9.16}$$

In equation (9.16) T denotes

$$T = \frac{\dfrac{\beta_i \delta^*}{U} \cdot \bar{\alpha}\delta^* . 10^6}{\dfrac{\beta_r \nu}{U^2} \cdot (\dfrac{U\delta^*}{\nu})^2} \tag{9.17}$$

and $\bar{x} = \dfrac{x}{c}$ where c is a constant reference length. The quantity T may be calculated as a function of $\bar{x}$ for a given value of $\dfrac{\beta_r \nu}{U^2}$ if the shape of the velocity profile and $\dfrac{U\delta^*}{\nu}$ are known as functions of $\bar{x}$. Moreover stability diagrams have to be known for the velocity profiles encountered.

The lower integration limit $\bar{x}_o$ in (9.16) denotes the value of $\bar{x}$ at which for the frequency considered $\dfrac{\beta_i \delta^*}{U} = 0$ for the first time.

9.3.   Some available stability diagrams.

As the stability calculations are rather laborious not many stability diagrams have been calculated. A review of these results may be found in [7], chapter 16 and [29], section IX; a selection of these results will be given below.

For the flat plate boundary layer without suction critical Reynoldsnumbers from different sources have been collected in table 9.1, stability diagrams are shown in fig. 9.3. It is seen that the results of various calculations show considerable differences. This is caused on the one hand by the different procedures followed for the stability calculations. On the other hand the Blasius profile has been approximated by different analytical expressions; in many cases the velocity profile for the flat plate boundary layer from some Pohlhausen type method has been used. Since these velocity profiles and especially their curvature may be different, the stability diagrams are not necessarily identical.

Some available stability diagrams for the plane stagnation point flow

without suction have been compared in fig. 9.4; again considerable
differences are shown.

Calculations for a whole series of Hartree profiles (see section 3.1.2)
have been made by Pretsch [96, 97, 98]. Stability diagrams are shown in
fig. 9.5; the critical Reynoldsnumber is given in fig. 9.6 as a function
of β. Figures 9.5 and 9.6 clearly show the stabilising influence of a
favourable pressure gradient $(\beta > 0)$. Also amplification calculations
have been made by Pretsch; these results will be discussed in more
detail in section 9.5.

The neutral stability curves for some cases with suction and blowing have
been calculated by Ulrich [99]. The flows considered are

    1. the flat plate with constant suction velocity

    2. the flat plate with $v_o \leadsto x^{-\frac{1}{2}}$

    3. the plane stagnation point with constant suction velocity.

The cirtical Reynoldsnumber is shown as a function of $\lambda_2 = \frac{-v_o}{U}\sqrt{\frac{Ux}{\nu}}$
in fig. 9.7 which clearly shows the strong stabilising influence of
suction. From the examples discussed in chapter 8 it is known that for
the boundary layer flows considered by Ulrich the velocity profile tends
to the asymptotic suction profile if the suction velocity $-v_o$ becomes
infinitely large $(\lambda_2 \rightarrow \infty)$. According to Ulrich's calculations the
critical Reynoldsnumber $\frac{U\delta^*}{\nu}$ becomes as high as 70000 for this case;
a recalculation by Freeman [100] gave 78000. Fig. 9.8 shows some
stability diagrams selected from Ulrich's results for different boundary
layer flows. This figure shows that if $(\frac{U\delta^*}{\nu})_{crit}$ is equal for two
different boundary layers also the remainder of the neutral stability
curve is roughly the same, irrespective of the pressure gradient or
suction velocity.

Comparison of this result with figs 9.3 and 9.4 reveals that the
stability diagrams calculated by different authors for the same flow
show as much variation as the stability diagrams obtained by the same
author for different velocity profiles with the same value of the
critical Reynoldsnumber.

In the remainder of the present work the amplification factor for
boundary layers with arbitrary pressure- and suction distributions will
be calculated. For this calculation stability diagrams including
information about the amplification rate at $\beta_i > 0$ have to be known.

To the best of the author's knowledge these results are only provided
by Pretsch's stability diagrams and it will be attempted to apply these
diagrams to arbitrary boundary layers.

In view of the comparisons of different stability diagrams made above,
the following procedure seems to be justified for assigning a stability
diagram to a certain velocity profile. From an approximate formula due
to Lin (section 9.4) the critical Reynoldsnumber is found. Then the
stability diagram from Pretsch's series with the same critical Reynolds
number is assumed to be valid for the velocity profile under
investigation. This implies that all possible stability diagrams are
considered to form a one-parameter family with the critical Reynoldsnumber
as parameter.

If only the critical Reynoldsnumber is needed a quick estimate may be
made using a formula of Wieghardt [101].

$$\left(\frac{U\delta^*}{\nu}\right)_{crit} = H \left(\frac{U\theta}{\nu}\right)_{crit} = H \, e^{26.3 - 8H} \tag{9.18}$$

where $H = \dfrac{\delta^*}{\theta}$. Fig. 9.9 shows that indeed equation (9.18) gives a
reasonably good approximation to the critical Reynoldsnumber for a
variety of boundary layers. For relatively strong suction however
Wieghardts relation seems to become invalid (Head, [63]); and it is
safer to use Lin's formula for all cases.

Since in boundary layer calculations using the momentum equation the
momentum loss thickness θ is the proper thickness parameter it is
advantageous in many cases to use a critical Reynoldsnumber based on θ.
From fig. 9.9 it follows that for the boundary layers, which have been
considered in the present section, equal values of H mean equal values
of $\left(\frac{U\theta}{\nu}\right)_{crit}$ and hence also of $\left(\frac{U\delta^*}{\nu}\right)_{crit}$. Therefore the comparisons of
the stability diagrams made in the present section can also be made
in terms of $\overline{\alpha}\theta$ and $\frac{U\theta}{\nu}$, instead of $\overline{\alpha}\delta^*$ and $\frac{U\delta^*}{\nu}$, without altering the
conclusions.

9.4.   Lin's formulae for the critical Reynoldsnumber.

A simple approximate formula for the calculation of the critical
Reynoldsnumber has been given by Lin [90], and reads

$$\left(\frac{Ud}{\nu}\right)_{crit} = \frac{25\left(\frac{\partial \bar{u}}{\partial y/d}\right)_o}{\bar{u}_c^4} \qquad (9.19)$$

In this equation d may be any length which is used to make the wall distance y non-dimensional.

$\bar{u}_c$ is the value of $\bar{u}$ for which the following equation is satisfied

$$-\pi \left(\frac{\partial \bar{u}}{\partial y/d}\right)_o \frac{\bar{u} \frac{\partial^2 \bar{u}}{\partial (y/d)^2}}{\left(\frac{\partial \bar{u}}{\partial y/d}\right)^3} = 0.58 \qquad (9.20)$$

For the momentum method discussed in chapter 5 it is appropriate to take $d = \sigma$ leading to $\frac{y}{d} = \eta$. Then equations (9.19) and (9.20) lead to

$$\left(\frac{U\Theta}{\nu}\right)_{crit} = \frac{25 \cdot \frac{\tau_o \sigma}{\mu U} \cdot \frac{\Theta}{\sigma}}{\bar{u}_c^4} \qquad (9.21)$$

and

$$\frac{-\bar{u} \frac{\partial^2 \bar{u}}{\partial \eta^2}}{\left(\frac{\partial \bar{u}}{\partial \eta}\right)^3} = \frac{0.58}{\pi \frac{\tau_o \sigma}{\mu U}} \qquad (9.22)$$

For the multimoment method given in chapter 7 it is useful to make d equal to δ as defined by equation (7.20). In that case (9.19) and (9.20) reduce to

$$\left(\frac{U\Theta}{\nu}\right)_{crit} = \frac{25 \sqrt{a_o}}{\bar{u}_c^4} \frac{\Theta}{x} \sqrt{\frac{Ux}{\nu}} \qquad (9.23)$$

$$\frac{-\bar{u} \frac{\partial s}{\partial \bar{u}}}{s \sqrt{s}} = \frac{1.16}{\pi \sqrt{a_o}} \qquad (9.24)$$

The equations (9.22) and (9.24) can easily be solved by iteration for a given velocity- or S-profile. It is even possible to include Lin's formulae in a computer program for the boundary layer calculation.

A comparison of results obtained with Lin's formulae and those from other calculations may be found in section IX of [29]. Some results for the flat plate boundary layer without suction have been collected in table 9.2. For the asymptotic suction profile the formula leads to

$(\frac{U\theta}{\nu})_{crit} = 40000$ or $\frac{U\delta^*}{\nu}_{crit} = 80000$ as compared to 70000 according

to Ulrich and 78000 obtained by Freeman. It follows from these comparisons that the accuracy of Lin's formula is quite satisfactory.

9.5.　Reduction of Pretsch's results to a form suitable for use on a digital computer.

Detailed stability calculations for some of the Hartree profiles have been made by Pretsch [96-98]. The stability diagrams are shown in fig. 9.5, while some characteristic parameters of the profiles have been collected in table 9.3. Stability diagrams for some other values of β have been obtained by Smith and Gamberoni [1] from interpolation in Pretsch's diagrams. In what follows these diagrams will be used to calculate the amplification factor σ_a. It follows from equation (9.16) that the only information needed from the diagrams is the quantity T as defined by (9.17). Values of T for a range of values of $\frac{\beta_r \nu}{U^2}$ and $\frac{U\delta^*}{\nu}$ have been obtained from Pretsch's work for $\beta = 1, 0.6, 0, -0.10$, -0.198 and for $\beta = 0.2, 0.1, -0.05$ from [1].

In fig. 9.10 for example the results are shown for the flat plate ($\beta = 0$) plotted as function of $^{10}\log \frac{U\theta}{\nu}$. It is seen from the figure that the curves for constant values of $\frac{\beta_r \nu}{U^2}$ may be approximated by parabola's of the form

$$T = T_o - K_1 \, (^{10}\log \frac{U\theta}{\nu} - K_2)^2 \qquad (9.25)$$

where the coefficients T_o, K_1 and K_2 depend on β and $\frac{\beta_r \nu}{U^2}$. Values for these coefficients have been obtained for all values of β and a range of values for $\frac{\beta_r \nu}{U^2}$. The results for $\beta = 0$ are shown in figure 9.11 as function of $^{10}\log \frac{\beta_r \nu}{U^2}$. The approximation given by (9.25) to the actual

values is shown in fig. 9.10. Finally cross plots have been made to find T_o, K_1 and K_2 as functions of β for constant values of $\dfrac{\beta_r \nu}{U^2}$. Since a unique relation exists between β and $(\dfrac{U\theta}{\nu})_{crit}$ (see fig. 9.6) it is possible to consider T_o, K_1 and K_2 as functions of $^{10}\log (\dfrac{U\theta}{\nu})_{crit}$.

Since it may be expected that Pretsch's results will not be very accurate, linear interpolation in $^{10}\log (\dfrac{U\theta}{\nu})_{crit}$ seems to be justified to find the coefficients of (9.25) for arbitrary values of $^{10}\log (\dfrac{U\theta}{\nu})_{crit}$. Table 9.4 gives T_o, K_1 and K_2 for different values of $\dfrac{\beta_r \nu}{U^2}$ at equidistant values of $^{10}\log (\dfrac{U\theta}{\nu})_{crit}$. The numbers quoted in the table have been chosen in such a way that by linear interpolation in $^{10}\log (\dfrac{U\theta}{\nu})_{crit}$ the values obtained from Pretsch's diagrams will be regained.

For convenience the reduced frequencies $\dfrac{\beta_r \nu}{U^2}$ have been denoted by a number f in table 9.4; results for intermediate values of $\dfrac{\beta_r \nu}{U^2}$ can be obtained by linear interpolation in the parameter f.

In view of the remarks made at the end of section 9.3 it will be assumed that table 9.4 can be applied to boundary layer flows with arbitrary suction- and pressure distributions.

9.6. Some existing methods for the calculation of the transition point.

In preceding sections it has been shown that it is possible to determine theoretically whether a particular boundary layer flow is stable or unstable. For instance for the flat plate the boundary layer becomes unstable as soon as $\dfrac{U\delta^{*}}{\nu}$ exceeds a critical value of about 575 corresponding to $\dfrac{Ux}{\nu} = 0.11 \times 10^6$. From experiments it is known however (see section 9.1) that actual transition starts at $\dfrac{Ux}{\nu} = 2.8 \times 10^6$ only. This means that a considerable distance will exist between the point of instability and the transition point.

From fig. 3.3 it follows that the instability has no direct effect on the friction drag; only when transition occurs the friction drag increases. It follows that for the calculation of the characteristics of airfoil sections it is important to possess a method for predicting

the possible occurrence of transition. Since the transition process is
not yet sufficiently understood these methods will necessarily be semi-
empirical in nature. Some of these methods are mentioned below.

In some methods the results of different transition measurements are
plotted in such a way that all points fall on a single curve. For a new
case transition may be "predicted" by assuming that the new case will
also fall on this universal curve. An important example of these methods
is due to Michel [106]. In his method $\frac{U\Theta}{\nu}$ at the transition point is plotted
versus the corresponding value of $\frac{Ux}{\nu}$; indeed results of different
experiments fall reasonably well on a single curve. The method is based
on experiments without suction and can not easily be generalised to
suction problems.

A different method has been given by Granville [107]. Here a universal
curve is obtained by plotting $(\frac{U\Theta}{\nu})_{tr} - (\frac{U\Theta}{\nu})_i$ versus the mean value $\overline{\Lambda_1}$
of the Pohlhausen parameter Λ_1, defined by

$$\overline{\Lambda}_1 = \frac{1}{\overline{x}_{tr} - \overline{x}_i} \int_{\overline{x}_i}^{\overline{x}_{tr}} \Lambda_1 \, d\overline{x} \tag{9.26}$$

The subscripts "tr" and "i" denote transition and instability respectively.
Another suggested method is to assume that transition occurs at a constant
value of $\frac{U\delta^*}{\nu}$. This results in a very rough estimate of the transition
point only.

To improve upon the above methods the determination of the transition
point should not be based on local quantities only but the history of
the boundary layer should be taken into account, since this determines
the amplification of unstable disturbances. Such a method has been
designed by the present author; it will be presented in the next section.

9.7. A new method for the semi-empirical determination of the transition region.

9.7.1. General.

It was shown by the present author in [3-5] and at the same time
independently by Smith and Gamberoni [1,2] that different experiments

on transition without suction can be correlated on the basis of the amplification factor σ_a. It was shown that the maximum value of σ_a which was reached at the transition position was roughly equal for all cases investigated. Hence in new cases an accurate estimate of the transition position may be found using the assumption that transition occurs as soon as the calculated value of $(\sigma_a)_{max}$ reaches this critical value. In the references cited above the method was shown to be valid for the no-suction case. It will be presented here in a modified form; furthermore it will be shown that the method is also applicable to cases with suction.

9.7.2. The amplification factor for the flat plate without suction.

Teh amplification factor σ_a is defined by equation (9.16)

$$\sigma_a = 10^{-6} \frac{U_\infty c}{\nu} \int_{\bar{x}_o}^{\bar{x}} T.\bar{U}\, d\bar{x} \tag{9.27}$$

If for the flat plate the reference velocity U_∞ and the reference length c are chosen as U and $\frac{\nu}{U}$ respectively, equation (9.27) reduces to

$$\sigma_a = 10^{-6} \int_{\frac{Ux_o}{\nu}}^{\frac{Ux}{\nu}} T\, d(\frac{Ux}{\nu}) \tag{9.28}$$

For the flat plate the relation between $\frac{U\theta}{\nu}$ and $\frac{Ux}{\nu}$ is known and it is possible to calculate σ_a for different frequencies $\frac{\beta_r \nu}{U^2}$ using table 9.4 and the formulae given in section 9.5. For this calculation a value of $(\frac{U\theta}{\nu})_{crit}$ has to be assumed; as some uncertainty exists here (see table 9.1) a range of values for the critical Reynoldsnumber has been used. For $(\frac{U\theta}{\nu})_{crit}$ = 260, which is the value obtained by Pretsch for $\beta = 0$, some results are shown in figs 9.12 and 9.13. Values of T are shown in fig. 9.12; the amplification factor σ_a is shown in fig. 9.13 where also the envelope giving the maximum amplification factor $(\sigma_a)_{max}$ has been drawn.

Similar calculations have been performed for other values of $(\frac{U\theta}{\nu})_{crit}$

from table 9.1; the results for $(\sigma_a)_{max}$ have been collected in fig.
9.14. Of course the calculation of the amplification factor can be
extended to arbitrary high Reynoldsnumbers. However, it is known from
experiments (see section 9.1) that transition sets in at $\frac{Ux}{\nu} = 2.8 \times 10^6$
and that the boundary layer is completely turbulent for $\frac{Ux}{\nu} > 3.9 \times 10^6$.
These limits have been inserted in fig. 9.14; it follows that to these
values of $\frac{Ux}{\nu}$ certain values of $(\sigma_a)_{max}$ correspond which are shown as
function of $(\frac{U\theta}{\nu})_{crit}$ in fig. 9.15 and table 9.5.

If Pretsch's value is used it is found that beginning and end of the
experimentally determined transition region correspond to $(\sigma_a)_{max} = 7.6$
and 9.7 respectively. In the earlier version of the method $\begin{bmatrix} 3-5 \end{bmatrix}$ the
values 7.8 and 10 were obtained. The slight differences with the present
values are easily explained by the fact that at that time only small
scale versions of Pretsch's charts were available to the author which
could not be read very accurately.

In most of the further calculations the momentum method of chapter 5
will be used in combination with Lin's formulae for the critical
Reynoldsnumber. Table 9.5 shows that this leads to $(\sigma_a)_{max} = 9.2$ and
11.2 at the beginning and end of the transition region
respectively. In what follows it will be shown that nearly the same
values are obtained for other boundary layers. It should be noted that
the linear stability theory has been used to calculate σ_a up till
transition. Of course not too much significance should be attached
to the details of these calculations. The maximum amplification factor
has to be considered only as a convenient parameter correlating
different factors which influence the transition.

9.7.3. The amplification factor for the EC 1440 airfoil section without suction.

For airfoil sections the boundary layer is not similar and hence for
different values of $\bar{x}$ different stability diagrams have to be used. If
$(\frac{U\theta}{\nu})_{crit}$ is known as a function of $\bar{x}$, for instance from Lin's formulae,
it is easily possible to calculate σ_a also for these cases using table
9.4.

In [3-5] results of transition measurements and calculations of the
amplification factor for the EC 1440 airfoil section have been presented.
In this work Pohlhausen's method was used for the boundary layer
calculations; critical Reynoldsnumbers for the velocity profiles were
found by relating Pohlhausen's λ to Hartree's β. This relation was
obtained by calculating the Hartree boundary layers for $U = u_1 \, x^{\frac{\beta}{2-\beta}}$
with Pohlhausen's method. The examples discussed in [3-5] will be
recalculated here using the momentum method of chapter 5 in combination
with Lin's formulae. Fig. 9.16 shows $\bar{U}$ as a function of $\bar{s}$ and the
results of the boundary layer calculations for different values of the
angle of attack α. Results of the amplification calculation for $\alpha = 0^{\circ}$
are shown in figs 9.17 and 9.18. Similar calculations have been
performed for other values of α; the results have been used to construct
fig. 9.19 where also the experimentally determined transition region
is shown. The curve $(\sigma_a)_{max} = 0$ in fig. 9.19 denotes the instability
point; it follows that both the instability point and transition move
forward with increasing angle of attack.

However, the distance between the instability point and transition can
be very large. If the beginning of transition is assumed to occur for
$(\sigma_a)_{max} = 9.2$ it may be seen from fig. 9.19 that the beginning of
transition is predicted accurately within 5°/o of the chord length for
$\alpha > -2^{\circ}$.

For $\alpha < -2^{\circ}$ transition is preceded by laminar separation; in this case
the distance between the predicted and actual positions where transition
starts may grow to 10°/o of the chord length.

Smith and Gamberoni [1,2] applied a similar analysis to a great number
of experimental data including results of free flight measurements.
They calculated the laminar boundary layer by means of a method which
for the flat plate produces Hartree's velocity profile for $\beta = 0$.
Hence, using Pretsch' value for the critical Reynoldsnumber, they should
find $(\sigma_a)_{max} = 7.6$ and 9.7 at the beginning and end of the transition
region. The conclusion of their analysis was that $(\sigma_a)_{max} = 9$ would
correlate the experimental data very well. Since no distinction was made

between beginning and end of the transition region the agreement with
the values 7.6 and 9.7 is very good. A difference between the present
method and the method of Smith and Gamberoni is that the last authors
calculate the amplification at constant values of $\frac{\beta_r \nu}{U_\infty^2}$ while for the
present method constant values of $\frac{\beta_r \nu}{U^2}$ are used. Since $\overline{U} = U/U_\infty$
does not change very much in the regions of interest and moreover only
the envelope of σ_a for different frequencies is used this difference
apparently has no effect on the results.

It has been mentioned already that the method becomes less accurate
if transition occurs close to or even downstream of the calculated
separation point. Some possible explanations for these discrepancies
are listed below.

1. Near separation the transition mechanism assumed in stability theory
   may not be the relevant one so that a method which is based on this
   theory may become less accurate.

2. Especially close to separation the shape of the calculated boundary
   layer velocity profiles may be in error so that a wrong value for
   $(\frac{U\theta}{\nu})_{crit}$ is found.

3. In cases where the critical Reynoldsnumber is low – which occurs close
   to separation – really nothing is known about the accuracy of Lin's
   formulae or Pretsch' stability diagrams.

4. There is no clear reason why the critical values of $(\sigma_a)_{max}$ at
   transition should be constants. An exact correspondence between
   experiment and theory for the results shown in fig. 9.19 might have
   been obtained for instance by assuming that the critical values are
   suitable functions of the critical Reynoldsnumber at transition.
   However, in further experiments no systematic variation of $(\sigma_a)_{max}$ with
   $(\frac{U\theta}{\nu})_{crit}$ at transition was found and hence in what follows constant
   critical values for $(\sigma_a)_{max}$ have been used.

9.7.4. The amplification factor for boundary layers with suction through a
porous surface.

Anticipating the results of an experimental investigation on the effects

of suction through a porous surface - to be described in chapter 11 -
it is stated here that the method is also applicable in the case of
suction.

9.8.   Some results for the flat plate with different suction laws.

9.8.1. The flat plate with constant suction velocity.

In section 8.11 the boundary layer on a flat plate with constant suction
velocity has been discussed. It was found that the non-dimensional
parameter $\Lambda_2 = \frac{-v_o \theta}{\nu}$ and the shape of the velocity profile only depend
on the variable $\bar{x}$ defined by

$$\bar{x} = (\frac{-v_o}{U})^2 \quad \frac{Ux}{\nu} \qquad (9.29)$$

Since the critical Reynoldsnumber depends on the shape of the velocity
profile only it also depends only on $\bar{x}$.

Values of $\frac{U\theta}{\nu}$ may be found as function of $\bar{x}$ for different values of the
suction coefficient $c_q = \frac{-v_o}{U}$ from

$$\frac{U\theta}{\nu} = \frac{\frac{-v_o \theta}{\nu}}{\frac{-v_o}{U}} \qquad (9.30)$$

Results of some calculations using the momentum method in combination
with Lin's formulae for the critical Reynoldsnumber, are shown in fig.
9.20. It follows that for $\frac{-v_o}{U} > 0.980 \times 10^{-4}$ nowhere along the length
of the plate $\frac{U\theta}{\nu}$ will exceed $(\frac{U\theta}{\nu})_{crit}$ and hence the boundary layer is
stable at all values of $\bar{x}$. For values of $\frac{-v_o}{U}$ less than 0.980×10^{-4}
the boundary layer becomes unstable in a certain interval.
A similar calculation has been made by Ulrich [99] using Iglisch' exact
solution for $\frac{U\theta}{\nu}$ and the results for $(\frac{U\theta}{\nu})_{crit}$ shown in figure 9.7. He
found that the suction coefficient c_q should exceed the value
1.18×10^{-4} to ensure a stable boundary layer for all values of $\bar{x}$. The
difference between the values 1.18 and 0.980 is easily explained by the
different procedures used to determine the critical Reynoldsnumber.

Fig. 9.21a and b show the drag of a flat plate with the constant
suction velocity $-v_o = 1.18 \times 10^{-4}$ U. Appendix 1 should be consulted for
an explanation of the terms "wake drag", "suction drag" and "total drag"
which are mentioned in figure 9.21. Included in the figure is the drag
for the flat plate without suction for both laminar and turbulent flow
(section 3.1.3). It is seen that the total drag with suction is higher
than for the Blasius boundary layer. However, it remains much smaller
than the drag of the flat plate with turbulent boundary layer which would
occur at high values of $\frac{Ux}{\nu}$ without suction.

The percentage reduction in total drag which would result from keeping
the boundary layer laminar is shown in figure 9.22. It follows that drag
reductions of 85 ^{o}/o will be possible at the value 25×10^6 for the
Reynoldsnumber $\frac{Ux}{\nu}$ which is representative for the wing of a modern jet
airliner in cruising flight.

The drag reduction shown in fig. 9.22 has been calculated on the
assumption of a constant suction velocity with such a magnitude that the
boundary layer remains stable along the full length of the plate. It may
be expected that less suction will be required if the boundary layer is
allowed to become unstable to such a degree that the maximum amplification
factor remains slightly below 9.2. This will be pursued further in the
remainder of the present section. A further reduction of the suction
quantity may be obtained by allowing the suction velocity to vary along
the length of the plate. This will be discussed further in section
9.8.2.

For the case of a constant suction velocity the amplification factor can
easily be calculated as follows.

If the definition (9.29) for $\bar{x}$ is used it is implied that the reference
length c has been defined as

$$c = \frac{U \nu}{(-v_o)^2} \tag{9.31}$$

If the reference speed U_∞ is made equal to the constant free stream
speed U then the Reynoldsnumber $R_c = \frac{U_\infty c}{\nu}$ becomes

$$R_c = \left(\frac{U}{-v_o}\right)^2 = c_q^{-2} \tag{9.32}$$

and equation (9.16) reduces to

$$\sigma_a = 10^{-6} \, c_q^{-2} \int_{\bar{x}_o}^{\bar{x}} T \, d\bar{x} \tag{9.33}$$

Results of amplification calculations for different values of c_q have been collected in fig. 9.23 where $(\sigma_a)_{max}$ is shown as function of $\bar{x}$. The peak value of the amplification factor is plotted in fig. 9.24 as function of c_q. If it is assumed that transition starts as soon as $(\sigma_a)_{max}$ reaches the critical value 9.2, then it may be concluded from fig. 9.24 that transition will not occur unless c_q falls below the value 0.485×10^{-4}. This value is only $50^o/o$ of the suction coefficient required to keep the boundary layer stable. Then it may be concluded that the suction coefficient can be much smaller than was assumed for the calculation of the drag reduction shown in fig. 9.22. This implies that the possible drag reduction may be much larger than shown in fig. 9.22.

Furthermore it should be noted that using a constant value of $-v_o$ results in a suction intensity which is too high at most stations on the plate. Only in the critical region this suction velocity is really necessary to prevent transition. To obtain a minimum suction quantity the suction velocity should be adjusted to the local needs of the boundary layer. This will be discussed further in section 9.8.2.

9.8.2. The flat plate with varying suction velocity.

Using the momentum method in combination with Lin's formulae for the critical Reynoldsnumber, it is easy to calculate the suction distribution which will maintain a neutrally stable boundary layer characterized by

$$\frac{U\theta}{\gamma} = \left(\frac{U\theta}{\gamma}\right)_{crit} \tag{9.34}$$

Since the momentum method and Lin's formulae lead to $\frac{U\theta}{\nu} = 0.661\sqrt{\frac{Ux}{\nu}}$

and $(\frac{U\theta}{\nu})_{crit}$ = 221 for the boundary layer on a flat plate without suction,

it follows that instability arises downstream of the position where

$\frac{Ux}{\nu} = 0.11 \times 10^6$. If suction is started at this point and the requirement

(9.34) is fulfilled, further downstream the suction distribution shown

in fig. 9.25 results. It may be seen from this figure that only locally

a high suction intensity is needed. For $\frac{Ux}{\nu} \rightarrow \infty$ the suction velocity

takes the constant value 0.125×10^{-4}U. This value easily follows from the

observation that for $\frac{Ux}{\nu} \rightarrow \infty$ the asymptotic suction profile is found

for which $\frac{-v_o\theta}{\nu} = 0.50$ and $(\frac{U\theta}{\nu})_{crit}$ = 40000 so that to satisfy equation

(9.34) the suction velocity should be given by

$$\frac{-v_o}{U} = \frac{\frac{-v_o\theta}{\nu}}{\frac{U\theta}{\nu}} = \frac{0.5}{4 \times 10^4} = 0.125 \times 10^{-4}$$

The total suction quantity obtained in this case is much less than for

the case of constant suction velocity. A further reduction will be

obtained if the amplification factor $(\sigma_a)_{max}$ is allowed to reach the

critical value 9.2. However, this will not be pursued further in the

present work.

Table 9.1: Critical Reynoldsnumber for the flat plate boundary layer.

$(\frac{U\delta^*}{\nu})_{crit}$	$(\frac{U\theta}{\nu})_{crit}$	$^{10}\log(\frac{U\theta}{\nu})_{crit}$	references
321	124	2.093	Timman et al [104]
420	162	2.210	Tollmien [105]
420	162	2.210	Lin [102]
480	185	2.268	Lin, equations 9.19 - 9.20
575	222	2.346	Ulrich [99]
645	249	2.396	Schlichting-Ulrich [115]
680	260	2.416	Pretsch, β=0 [96]

Table 9.2: Results of Lin's formulae for different approximation to the velocity
profile on a flat plate.

$(\frac{U\delta^*}{\nu})_{crit}$	$(\frac{U\theta}{\nu})_{crit}$	$^{10}\log(\frac{U\theta}{\nu})_{crit}$	Velocity profile
480	185	2.268	exact
577	221	2.345	momentum method
754	310	2.492	multimoment method N = 5
493	196	2.292	" " N = 6
508	200	2.301	" " N = 7
519	203	2.307	" " N = 8
498	194	2.288	" " N = 9

Table 9.3: Characteristic parameters of the Hartree velocity profiles including the
critical Reynoldsnumber according to Pretsch.

β	H	$(\frac{U\delta^*}{\nu})_{crit}$	$(\frac{U\theta}{\nu})_{crit}$	$^{10}\log(\frac{U\delta^*}{\nu})_{crit}$	$^{10}\log(\frac{U\theta}{\nu})_{crit}$
1	2.22	12400	5603	4.094	3.748
0.6	2.27	8640	3795	3.936	3.579
0.2	2.41	2955	1225	3.471	3.088
0.1	2.48	1658	669	3.219	2.825
0	2.59	680	260	2.832	2.416
-0.05	2.67	354	133	2.549	2.123
-0.10	2.80	126	45	2.100	1.654
-0.198	4.03	0	0	-	-

Table 9.4: Coefficients of equation (9.25) obtained from Pretsch' diagrams.

$10\log(\frac{U\theta}{\nu})_{crit}$	$f=1$ $\frac{\beta_r \nu}{u^2} = 10^{-6}$			$f=2$ $\frac{\beta_r \nu}{u^2} = 2.5\ 10^{-6}$			$f=3$ $\frac{\beta_r \nu}{u^2} = 5.10^{-6}$		
	T_o	K_1	K_2	T_o	K_1	K_2	T_o	K_1	K_2
1	.04	6.00	4.270	13.05	116.00	3.750	25.60	169	3.115
1.5	.75	0	4.200	8.00	87.00	3.670	15.10	136	3.250
2	1.20	10.50	3.988	2.95	58.00	3.590	4.60	105	3.385
2.5	.55	10.50	3.800	.81	21.50	3.578	1.10	35	3.390
3	.22	10.50	3.900	.40	21.50	3.640	.80	35	3.450
3.5	.22	10.50	4.000	.23	30.00	3.731	0	35	3.510
4	.22	16.00	4.100	-022	38.50	3.825	-0.80	35	3.570

$10\log(\frac{U\theta}{\nu})_{crit}$	$f=4$ $\frac{\beta_r \nu}{u^2} = 7.5\ 10^{-6}$			$f=5$ $\frac{\beta_r \nu}{u^2} = 10^{-5}$			$f=6$ $\frac{\beta_r \nu}{u^2} = 2.5\ 10^{-5}$		
	T_o	K_1	K_2	T_o	K_1	K_2	T_o	K_1	K_2
1	33.80	212	3.020	39.90	245	2.966	62.70	401	2.790
1.5	19.70	180	3.140	23.10	213	3.068	36.60	365.5	2.845
2	5.60	148.5	3.260	6.30	181	3.170	10.50	331	2.900
2.5	1.55	54	3.270	2.15	76	3.200	3.90	196	2.945
3	1.10	44	3.338	1.10	54	3.260	-0.10	51.5	3.030
3.5	-0.275	44	3.402	-0.735	33	3.315	-4.10	0	3.113
4	-1.10	44	3.466	-2.40	11	3.370	-8.10	0	3.196

$10\log(\frac{U\theta}{\nu})_{crit}$	$f=7$ $\frac{\beta_r \nu}{u^2} = 5.10^{-5}$			$f=8$ $\frac{\beta_r \nu}{u^2} = 7.5\ 10^{-5}$			$f=9$ $\frac{\beta_r \nu}{u^2} = 10^{-4}$		
	T_o	K_1	K_2	T_o	K_1	K_2	T_o	K_1	K_2
1	83.40	890	2.660	104.00	1224	2.560	125.80	1720	2.480
1.5	50.50	685	2.660	63.10	921	2.560	74.00	1234	2.480
2	17.60	480	2.700	21.20	620	2.570	22.20	760	2.490
2.5	3.30	345	2.750	1.40	511	2.640	0	705	2.555
3	- 1.60	200	2.850	- 1.10	400	2.710	- 1.10	650	2.625
3.5	- 6.50	60	2.950	- 3.60	300	2.780	- 2.20	600	2.695
4	-11.40	0	3.050	- 6.10	200	2.850	- 3.30	550	2.765

Table 9.4: (continued)

$10 \log(\frac{U\theta}{\nu})_{crit}$	f = 10 $\frac{\beta_r \nu}{U^2} = 2.5 \ 10^{-4}$			f = 11 $\frac{\beta_r \nu}{U^2} = 5.10^{-4}$			f = 12 $\frac{\beta_r \nu}{U^2} = 7.5 \ 10^{-4}$		
	T_o	K_1	K_2	T_o	K_1	K_2	T_o	K_1	K_2
1	182.00	3025	2.240	218.80	4215	2.040	213	4930	1.945
1.5	100.50	1965	2.240	111.40	2670	2.040	104.5	3120	1.945
2	19.00	880	2.240	4.00	1800	2.040	- 4	1330	1.945
2.5	- 7.70	845	2.400	-103.40	1045	2.040	- 4	0	1.945
3	- 7.70	810	2.560	-103.40	200	2.040	- 4	0	1.945
3.5	- 7.70	770	2.720	-103.40	0	2.040	- 4	0	1.945
4	- 7.70	730	2.880	-103.40	0	2.040	- 4	0	1.945

$10 \log(\frac{U\theta}{\nu})_{crit}$	f = 13 $\frac{\beta_r \nu}{U^2} = 10^{-3}$		
	T_o	K_1	K_2
1	202.80	5350	1.865
1.5	95.40	3475	1.865
2	- 12	1560	1.865
2.5	- 12	0	1.865
3	- 12	0	1.865
3.5	- 12	0	1.865
4	- 12	0	1.865

Table 9.5: Amplification factors at transition for the flat plate without suction.

Value assumed for		$(\sigma_a)_{max}$ at the experimentally determined transition region	
$10 \log(\frac{U\theta}{\nu})_{crit}$	$(\frac{U\theta}{\nu})_{crit}$	beginning	end
2.416	260	7.6	9.7
2.345	222	9.2	11.2
2.268	185	11.0	12.8
2.093	124	15.0	16.8
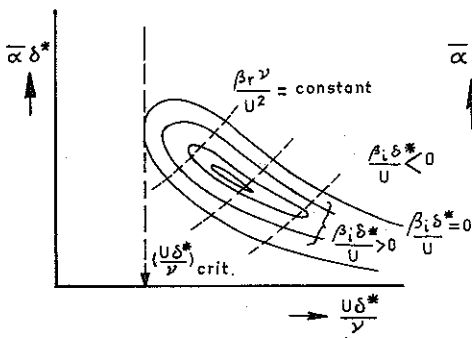
FIG.9.1: STABILITY DIAGRAM
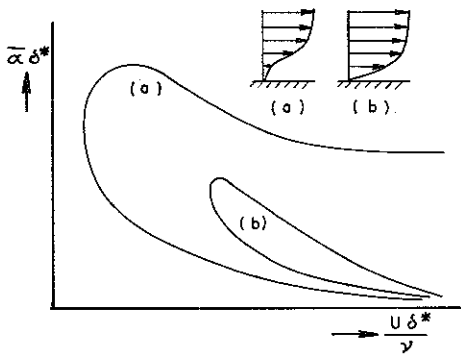
FIG.9.2: INFLUENCE OF SHAPE OF
VELOCITY PROFILE ON STABILITY DIAGRAM

LIN [102]
SHEN [103]
TIMMAN et al. [104]
TOLLMIEN [105]
PRETSCH [96]
ULRICH [99]
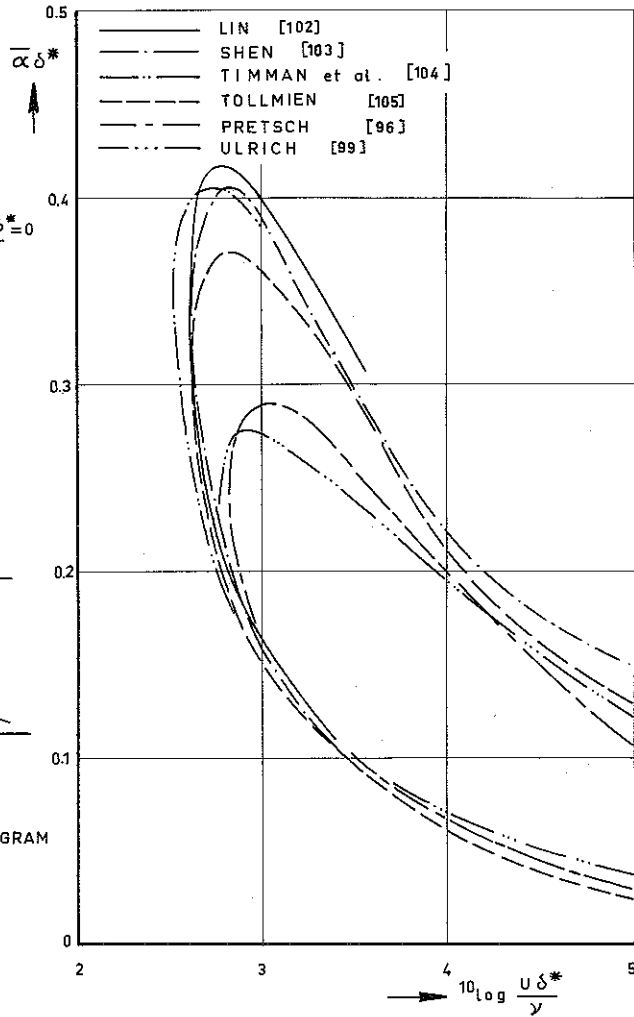
FIG.9.3: NEUTRAL STABILITY CURVES FOR THE FLAT
PLATE WITHOUT SUCTION FROM DIFFERENT SOURCES.

Pretsch

Ulrich
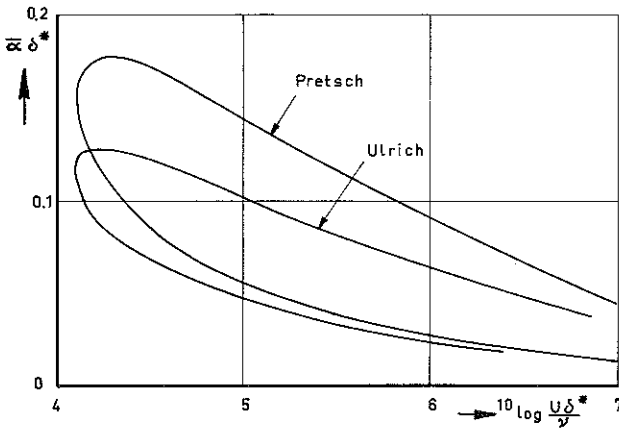
FIG. 9.4 : NEUTRAL STABILITY CURVES
FOR THE PLANE STAGNATION POINT
WITHOUT SUCTION.
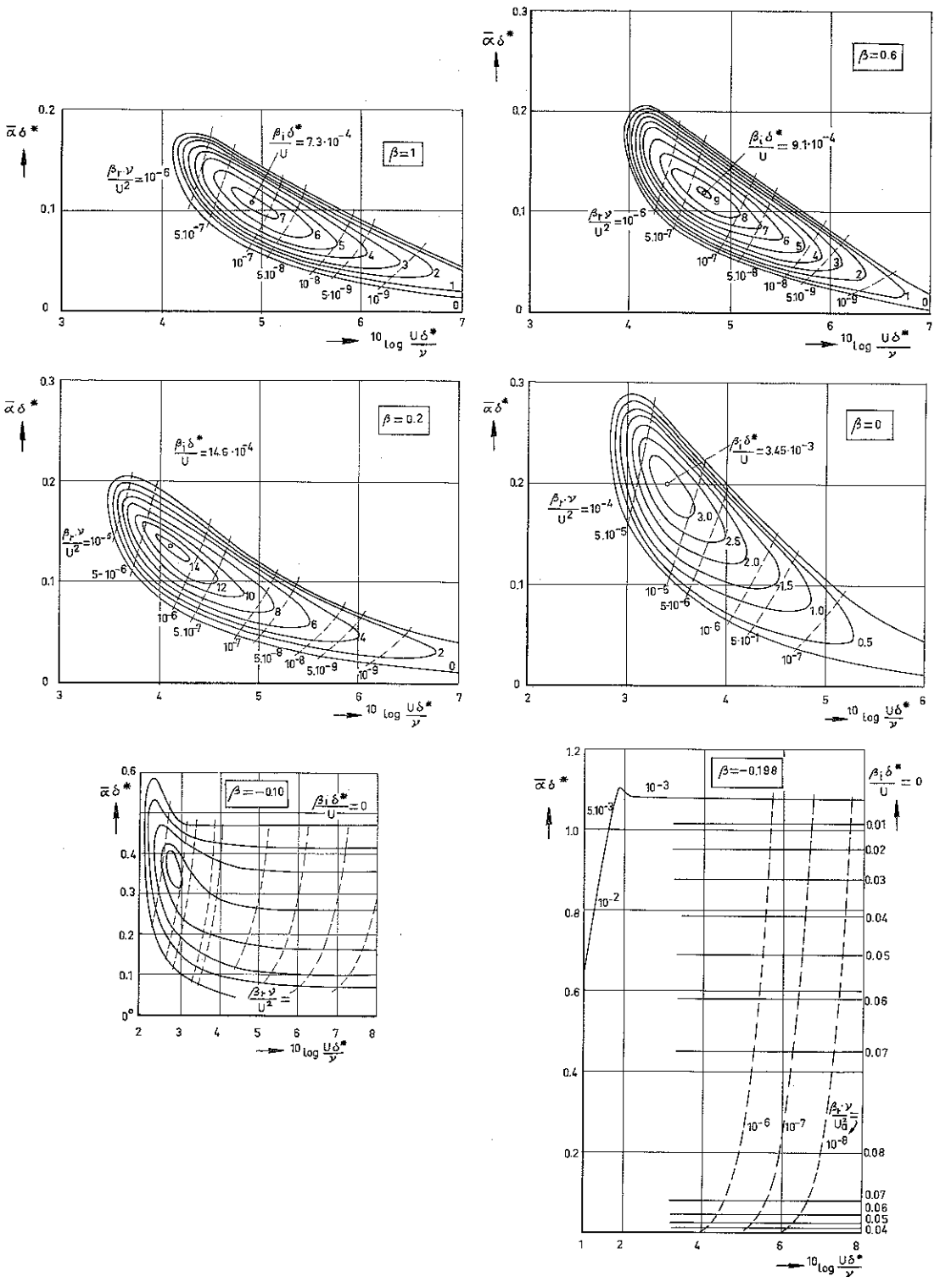
FIG. 9.5: PRETSCH'S DIAGRAMS FOR SOME HARTREE PROFILES.
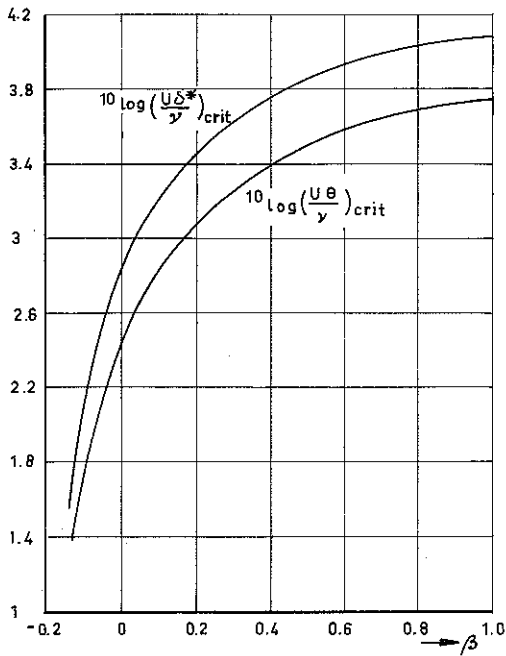
FIG. 9.6: CRITICAL REYNOLDS NUMBERS FOR THE HARTREE PROFILES ACCORDING TO PRETSCH.

Figure 9.6 axes labels: vertical ticks 4.2, 3.8, 3.4, 3, 2.6, 2.2, 1.8, 1.4, 1; curves labeled $^{10}\log\left(\frac{U\delta^*}{\nu}\right)_{crit}$ and $^{10}\log\left(\frac{U\theta}{\nu}\right)_{crit}$; horizontal axis -0.2, 0, 0.2, 0.4, 0.6, 0.8, 1.0, β.
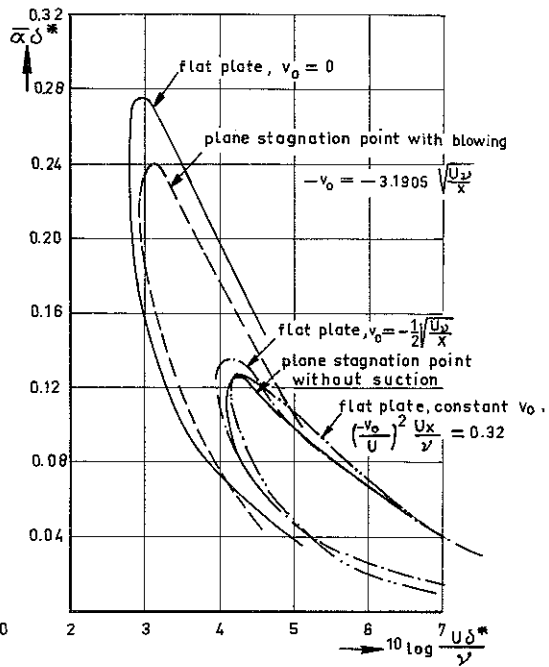
FIG. 9.8: SOME NEUTRAL STABILITY CURVES FOR DIFFERENT BOUNDARY LAYERS ACCORDING TO ULRICH.

Figure 9.8 labels: vertical axis $\overline{\alpha}\delta^*$ with ticks 0.32, 0.28, 0.24, 0.20, 0.16, 0.12, 0.08, 0.04. Curve labels: "flat plate, $v_0 = 0$"; "plane stagnation point with blowing $-v_0 = -3.1905\sqrt{\frac{U\nu}{x}}$"; "flat plate, $v_0 = -\frac{1}{2}\sqrt{\frac{U\nu}{x}}$"; "plane stagnation point without suction"; "flat plate, constant v_0, $\left(-\frac{v_0}{U}\right)^2\frac{Ux}{\nu} = 0.32$". Horizontal axis 2, 3, 4, 5, 6, 7 $^{10}\log\frac{U\delta^*}{\nu}$.
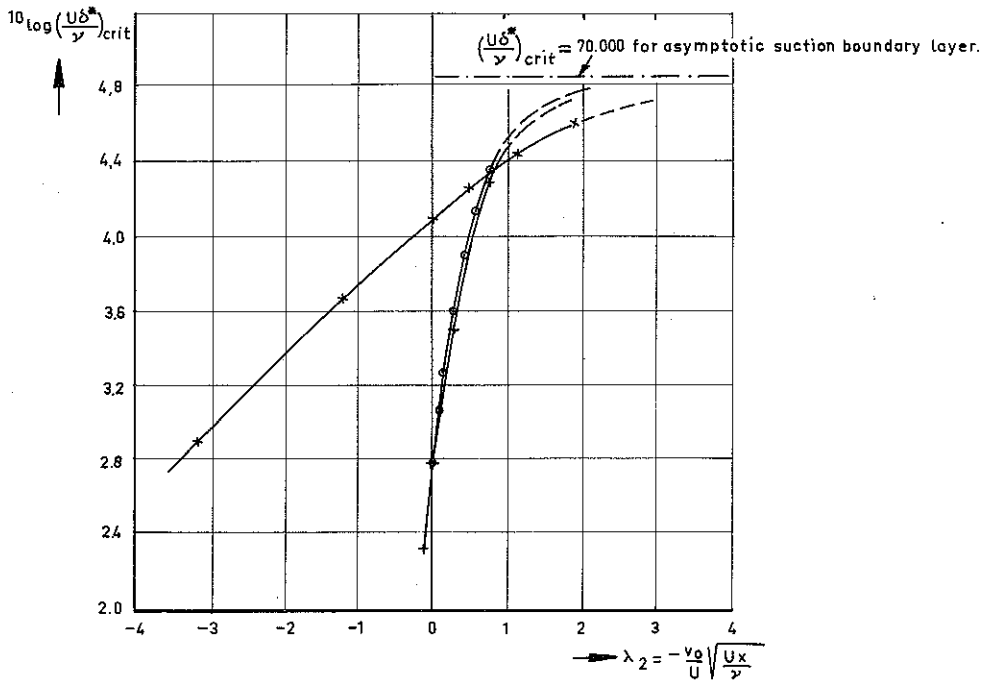
FIG. 9.7: CRITICAL REYNOLDSNUMBERS FOR SOME BOUNDARY LAYER FLOWS WITH SUCTION ACCORDING TO ULRICH

Figure 9.7 labels: vertical axis $^{10}\log\left(\frac{U\delta^*}{\nu}\right)_{crit}$ with ticks 4,8; 4,4; 4,0; 3,6; 3,2; 2,8; 2,4; 2,0. Note: $\left(\frac{U\delta^*}{\nu}\right)_{crit} = 70.000$ for asymptotic suction boundary layer. Horizontal axis -4, -3, -2, -1, 0, 1, 2, 3, 4; $\lambda_2 = -\frac{v_0}{U}\sqrt{\frac{Ux}{\nu}}$.

Legend:
- ——o—— flat plate, v_0 constant
- ——+—— flat plate, $v_0 \sim x^{-\frac{1}{2}}$
- ——x—— plane stagnation point, v_0 constant.
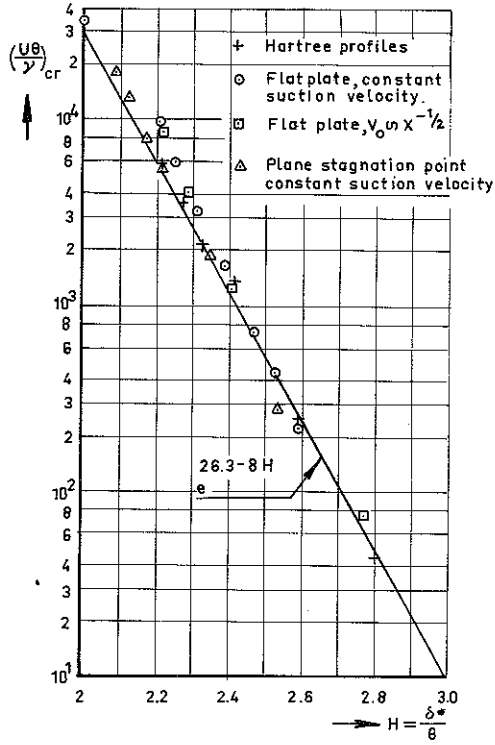
FIG. 9.9 : $\left(\dfrac{U\theta}{\nu}\right)_{crit}$ FOR SOME BOUNDARY LAYERS WITH AND
WITHOUT SUCTION.
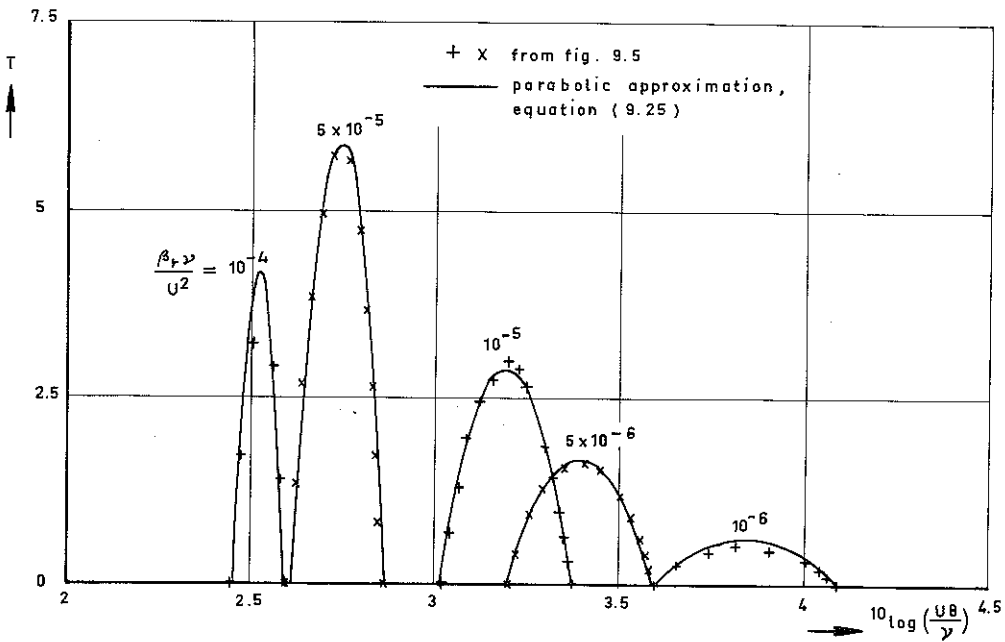
FIG. 9.10 : THE FUNCTION T FOR $\beta = 0$ AS DEFINED BY EQUATION (9.17)
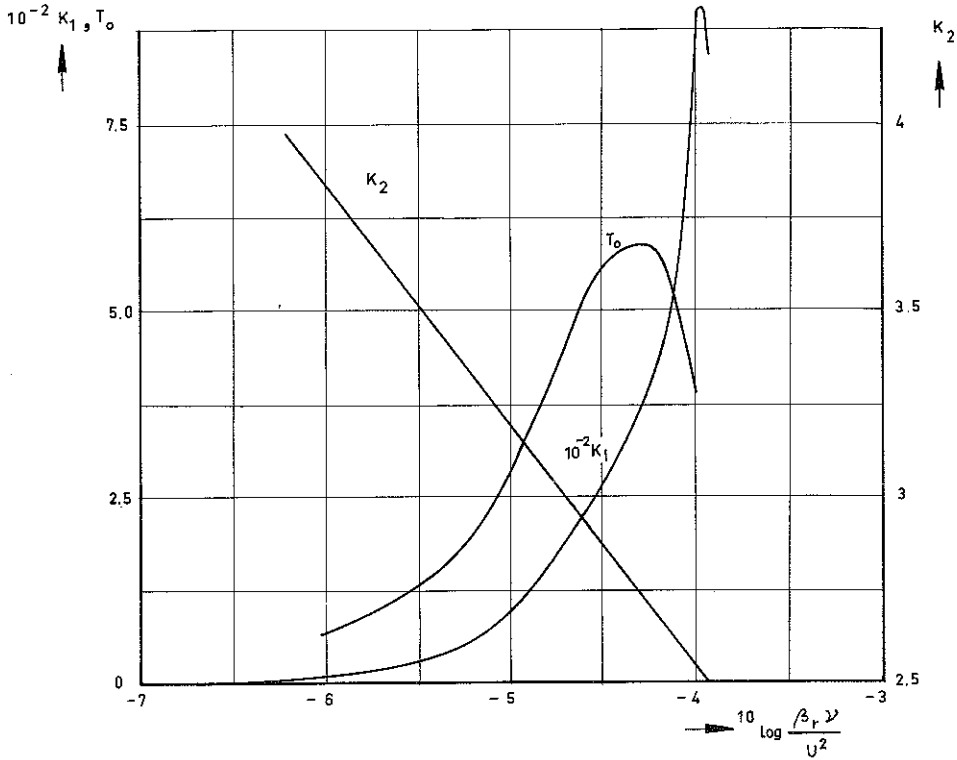
FIG. 9.11: COEFFICIENTS IN EQUATION (9.25) FOR $\beta = 0$.
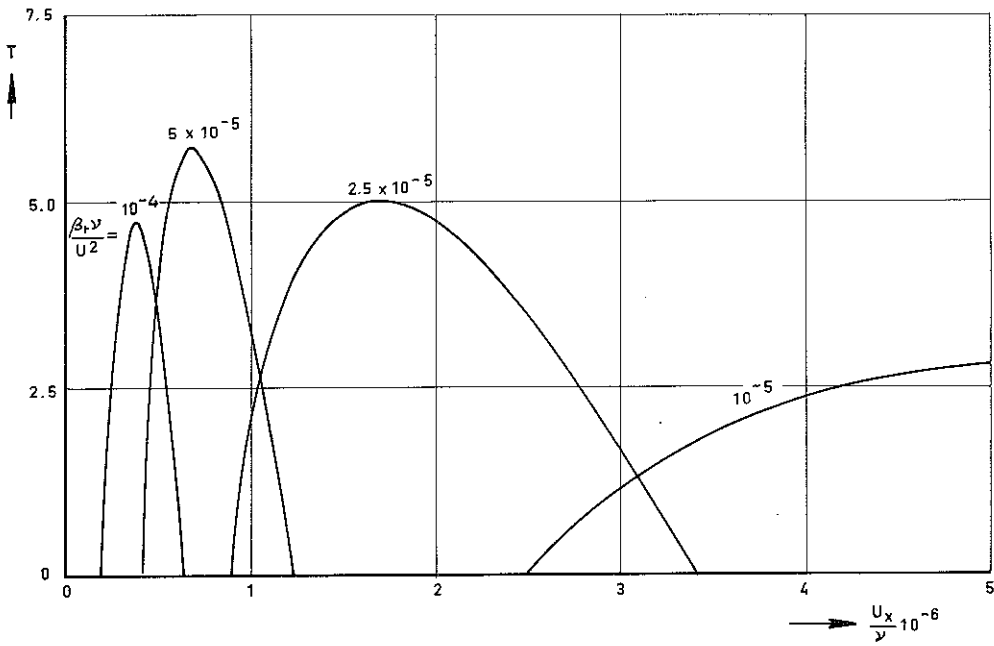
FIG. 9.12 : AMPLIFICATION RATE T FOR THE FLAT PLATE ($\beta = 0$)

FIG. 9.13: AMPLIFICATION FACTOR σ_a FOR THE FLAT PLATE $(\beta = 0)$ ⟶ $\frac{Ux}{\nu} 10^{-6}$

FIG. 9.14: MAXIMUM AMPLIFICATION FACTOR FOR THE FLAT PLATE
WITHOUT SUCTION AT DIFFERENT VALUES ASSUMED FOR $\left(\frac{U\theta}{\nu}\right)_{crit}$.
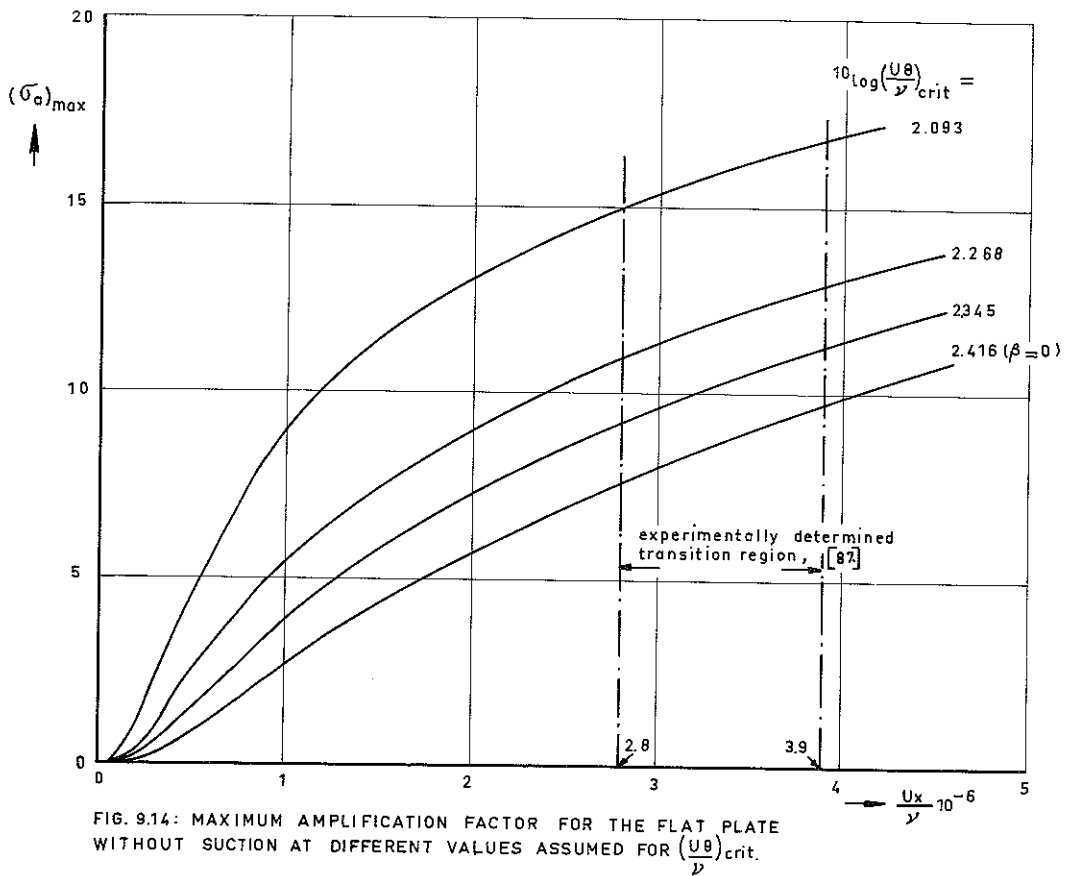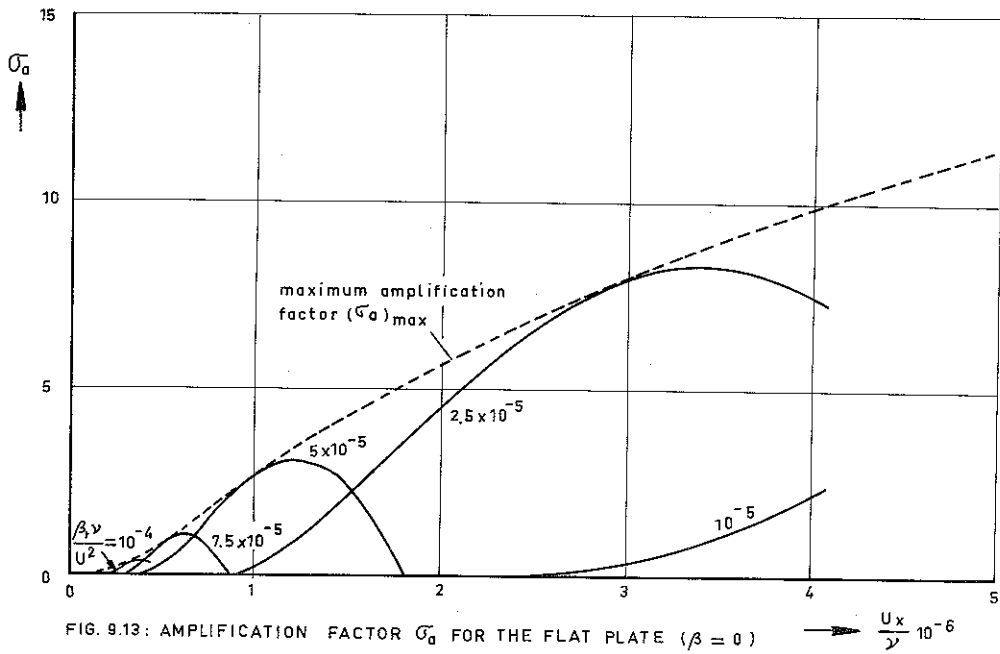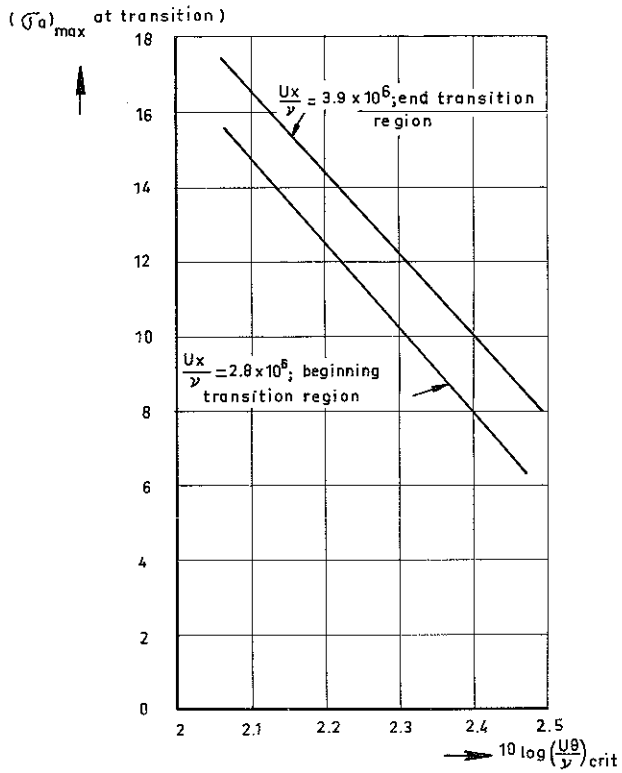
FIG. 9.15 : CROSS PLOT FROM FIG. 9.14.
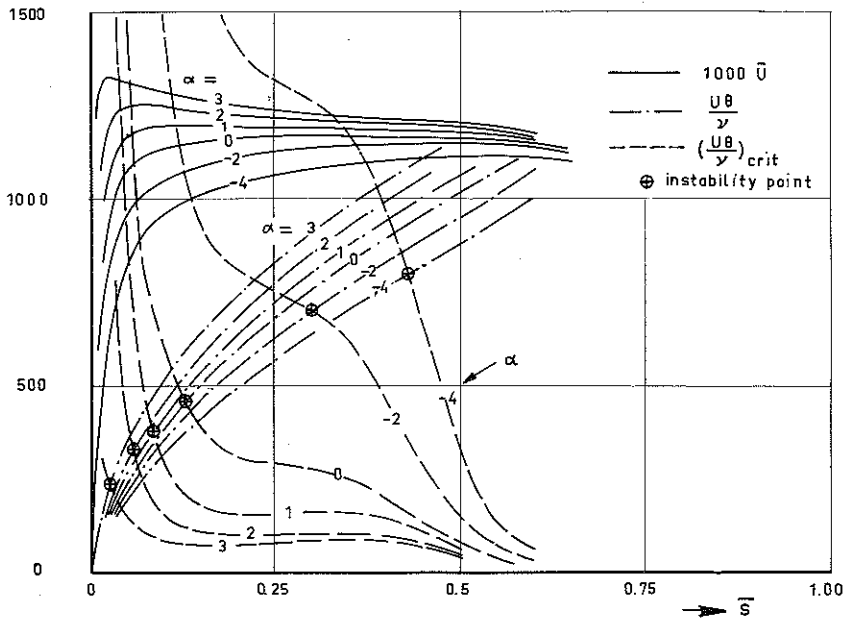
FIG. 9.16 : RESULTS OF THE MOMENTUM METHOD FOR THE EC 1440 AIRFOIL SECTION;
$R_c = 4.35 \times 10^6$.
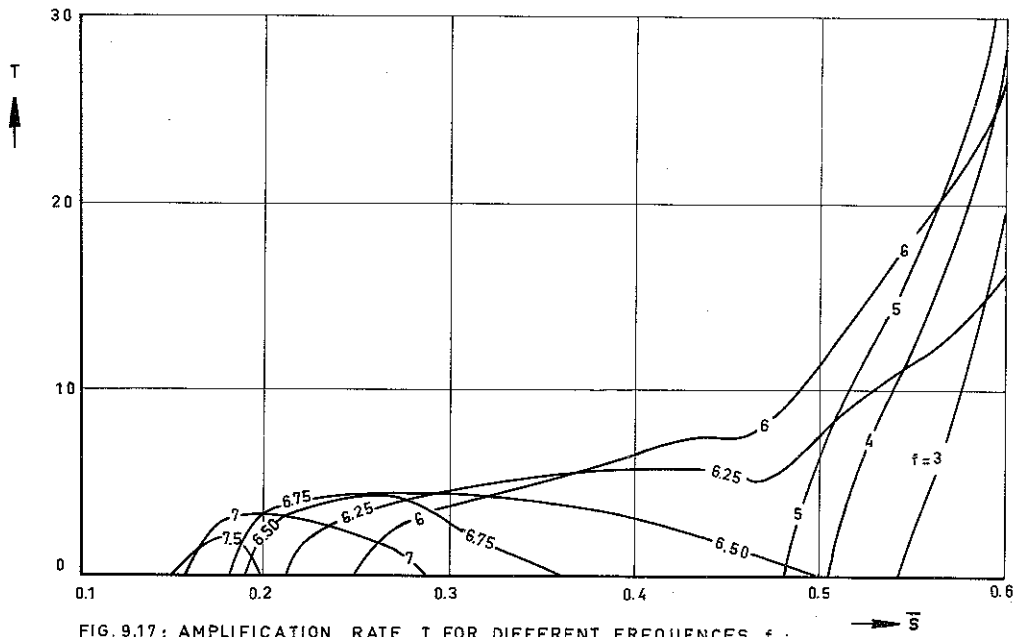
FIG. 9.17: AMPLIFICATION RATE T FOR DIFFERENT FREQUENCES f ;
EC 1440 AIRFOIL SECTION ; $\alpha = 0$, $R_c \simeq 4.35 \times 10^6$.
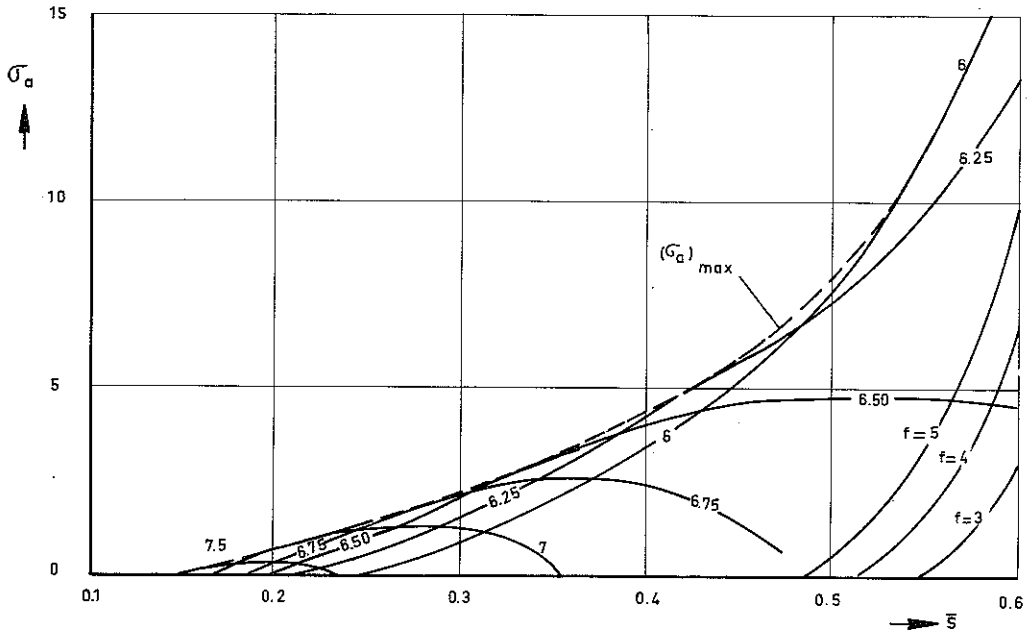
FIG. 9.18: AMPLIFICATION FACTOR FOR DIFFERENT FREQUENCES f ;
EC 1440 AIRFOIL SECTION ; $\alpha = 0$, $R_c = 4.35 \times 10^6$.
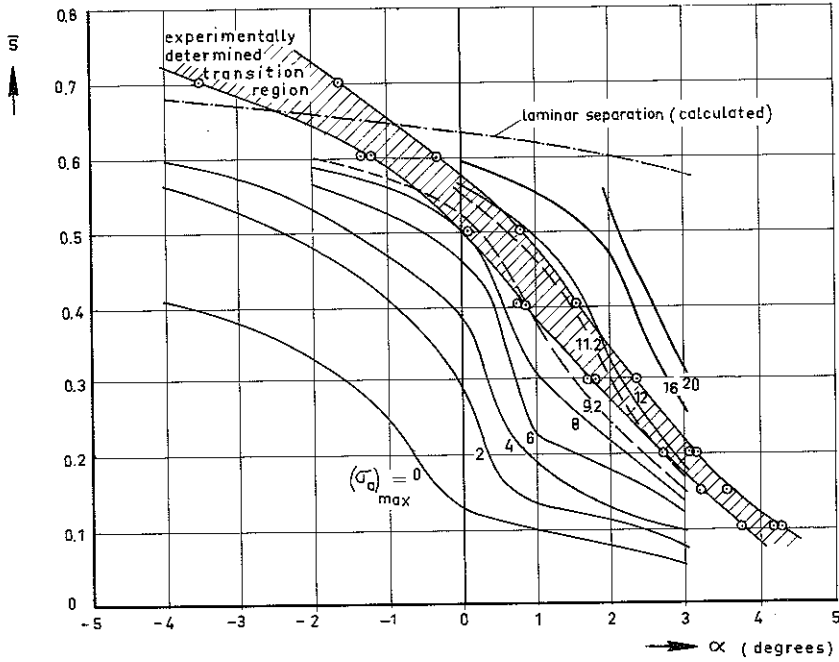
FIG.9.19 : CALCULATED AMPLIFICATION FACTOR AND MEASURED
TRANSITION REGION FOR THE EC 1440 AIRFOIL SECTION.
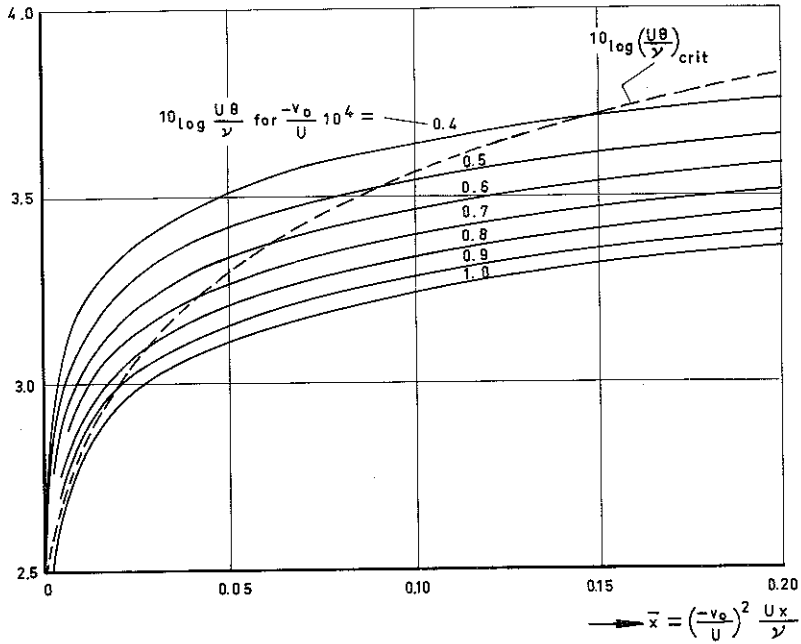
FIG.9.20: FLAT PLATE WITH CONSTANT SUCTION VELOCITY :
$^{10}\log\left(\frac{U\theta}{\nu}\right)_{crit}$ AND $^{10}\log\frac{U\theta}{\nu}$ FOR DIFFERENT SUCTION COEFFICIENTS.

$^{10}\log c_d$

-2

turbulent without suction

"natural transition"

$c_{df} = \dfrac{0.455}{(\log R_c)^{2.58}} - \dfrac{9220}{R_c}$

-3

③

②

Laminar without suction

-4

①

-5

5 6 7 8 $^{10}\log \dfrac{UX}{y}$ 9

(a) logarithmic scale for c_d

c_d

.0075

.0050

Laminar without suction

turbulent without suction

.0025

natural transition

① ② ③

0

5 6 7 8 $^{10}\log \dfrac{UX}{y}$ 9

(b) linear scale for c_d
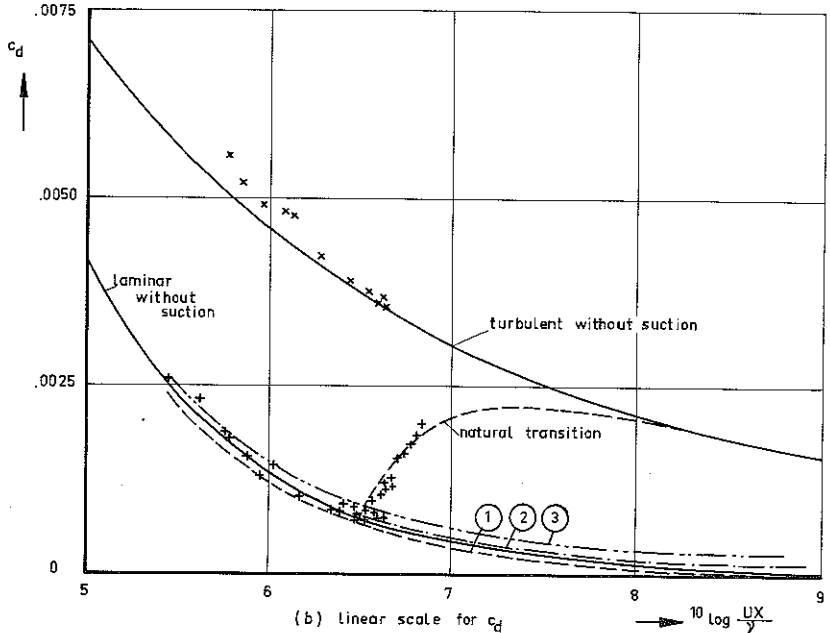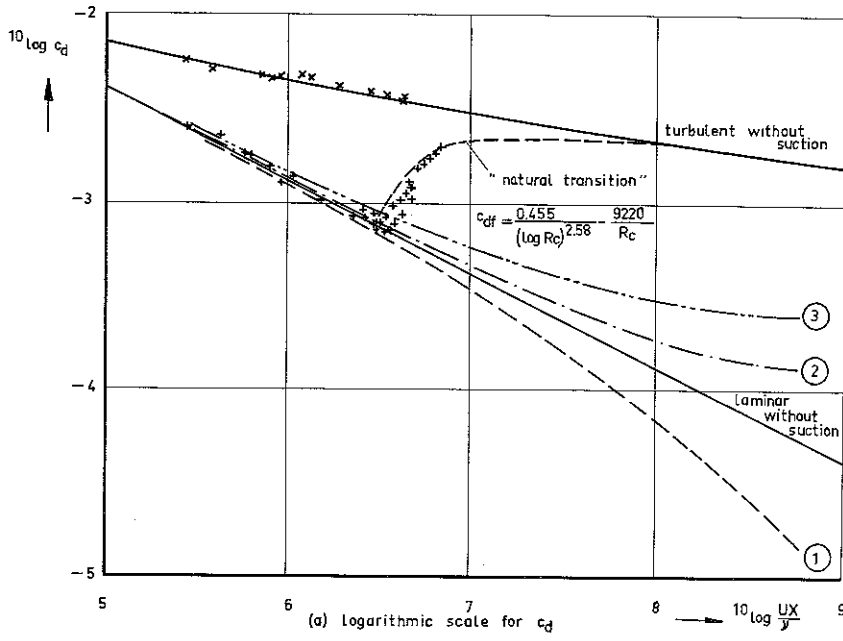
FIG. 9.21: DRAG COEFFICIENT OF FLAT PLATE WITH CONSTANT SUCTION VELOCITY

$+$ experimental results, smooth plate

$\times$,, ,, , trip wire near leading edge } no suction

—— turbulent without suction, Schlichting, $c_{df} = \dfrac{0.455}{(\log R_c)^{2.58}}$

—— laminar without suction, Blasius, $c_{df} = 1.328 \left(\dfrac{UX}{y}\right)^{-0.50}$

① ––– laminar, $c_q = \dfrac{-V_0}{U} = 1.18 \times 10^{-4}$, wake drag only, $c_d = 2\dfrac{\theta}{X}$

② –·–·– ,, ,, , wake drag + ideal suction drag $c_d = 2\dfrac{\theta}{X} + c_q$

③ –··–··– ,, ,, , friction drag, $c_{df} = 2\dfrac{\theta}{X} + 2c_q$
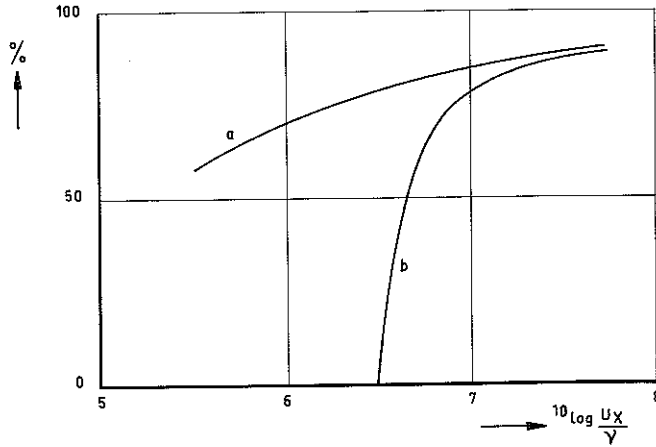
FIG.9.22: REDUCTION OF TOTAL DRAG FOR THE FLAT PLATE WITH CONSTANT
SUCTION VELOCITY ; $\frac{-v_0}{U} = 1.18 \times 10^{-4}$

(a): WITH RESPECT TO THE FULLY TURBULENT BOUNDARY LAYER
WITHOUT SUCTION

(b): WITH RESPECT TO THE BOUNDARY LAYER FOR "NATURAL TRANSITION"
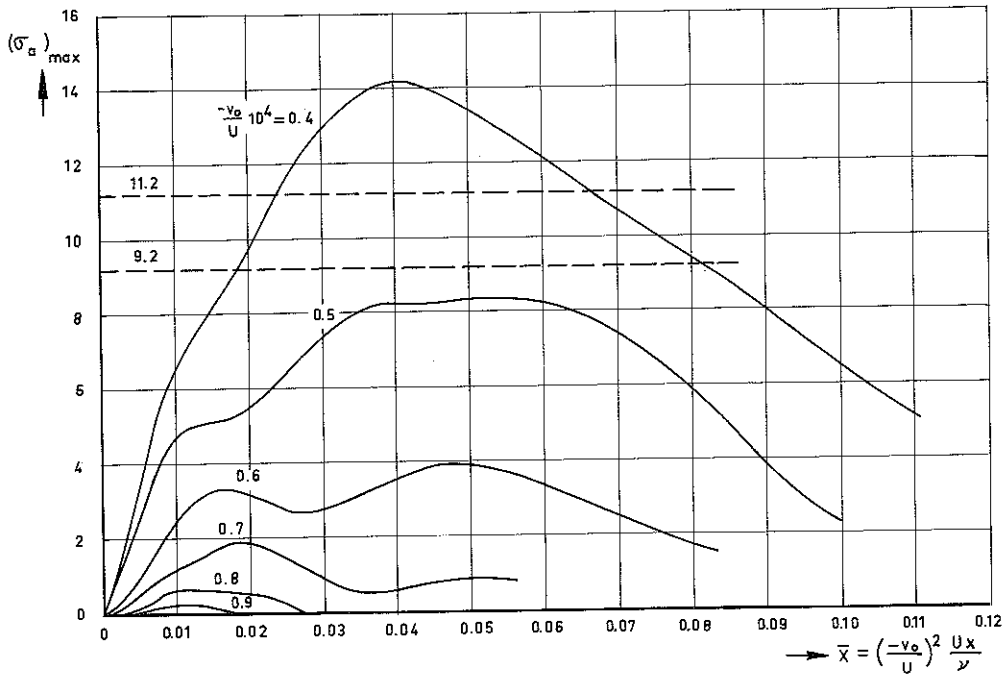
FIG.9.23: MAXIMUM AMPLIFICATION FACTOR FOR THE FLAT PLATE WITH CONSTANT SUCTION
VELOCITY AT DIFFERENT SUCTION FLOW COEFFICIENTS.
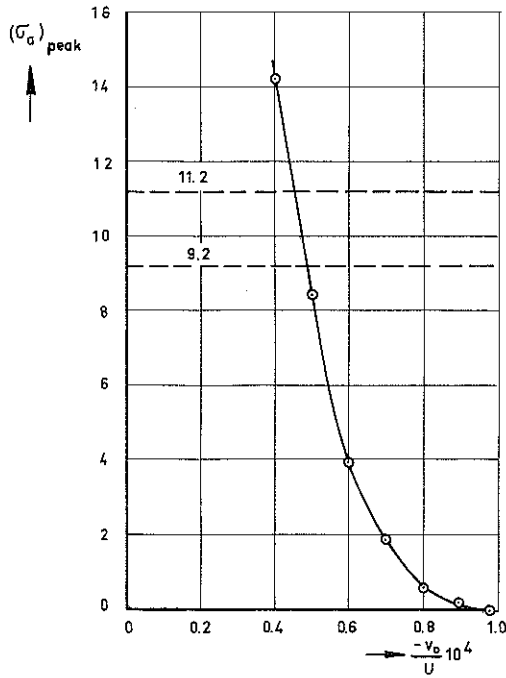
FIG.9.24.: CROSS PLOT FROM FIG.9.23; PEAK AMPLIFICATION FACTOR
FOR THE FLAT PLATE WITH CONSTANT SUCTION VELOCITY.
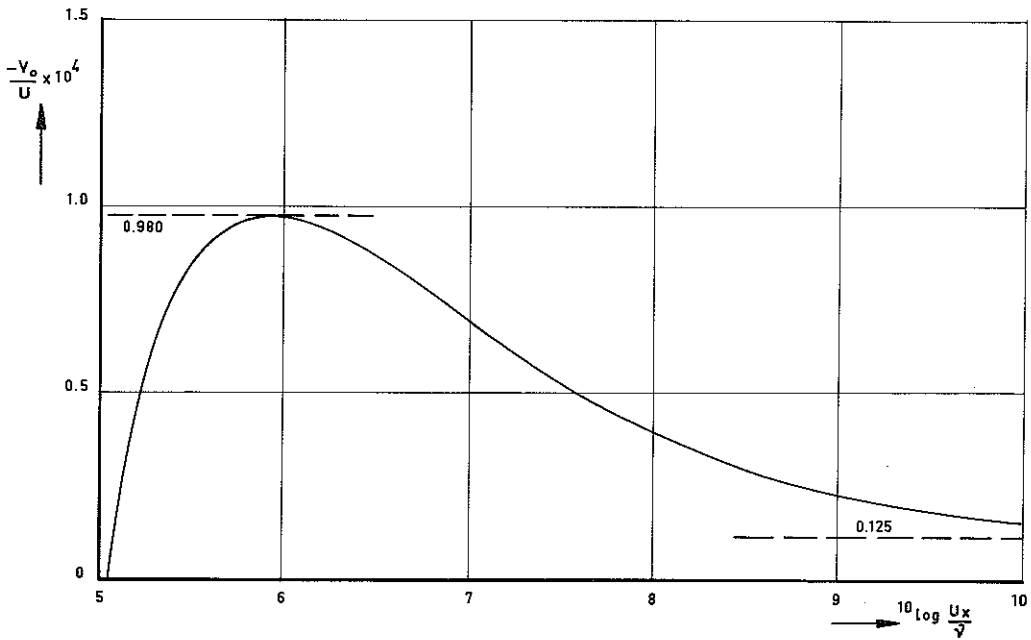
FIG.9.25: SUCTION DISTRIBUTION REQUIRED FOR THE FLAT PLATE TO MAINTAIN A NEUTRALLY STABLE
BOUNDARY LAYER DOWNSTREAM OF THE INSTABILITY POINT.